Nano Research

ISSN 1998-0124 CN 11-5974/O4
https://doi.org/10.26599/NR.2026.94908835

Review Article

Edge-rich carbon-based single-atom catalysts: Recent progress and critical contributions to electrocatalytic applications

Chenghong Hu, Yuwei Wang, Hafiz Muhammad Adeel Sharif, Yang Cai, Linxiao Hou, Xuelei Yan, Changping Li(✉)
Research Center for Eco-Environmental Engineering, Dongguan University of Technology, Dongguan 523808, China

Nano Res., **Just Accepted Manuscript** • https://doi.org/10.26599/NR.2026.94908835
https://www.sciopen.com/journal/1998-0124 on May. 12, 2026

Just Accepted

TABLE OF CONTENTS (TOC)

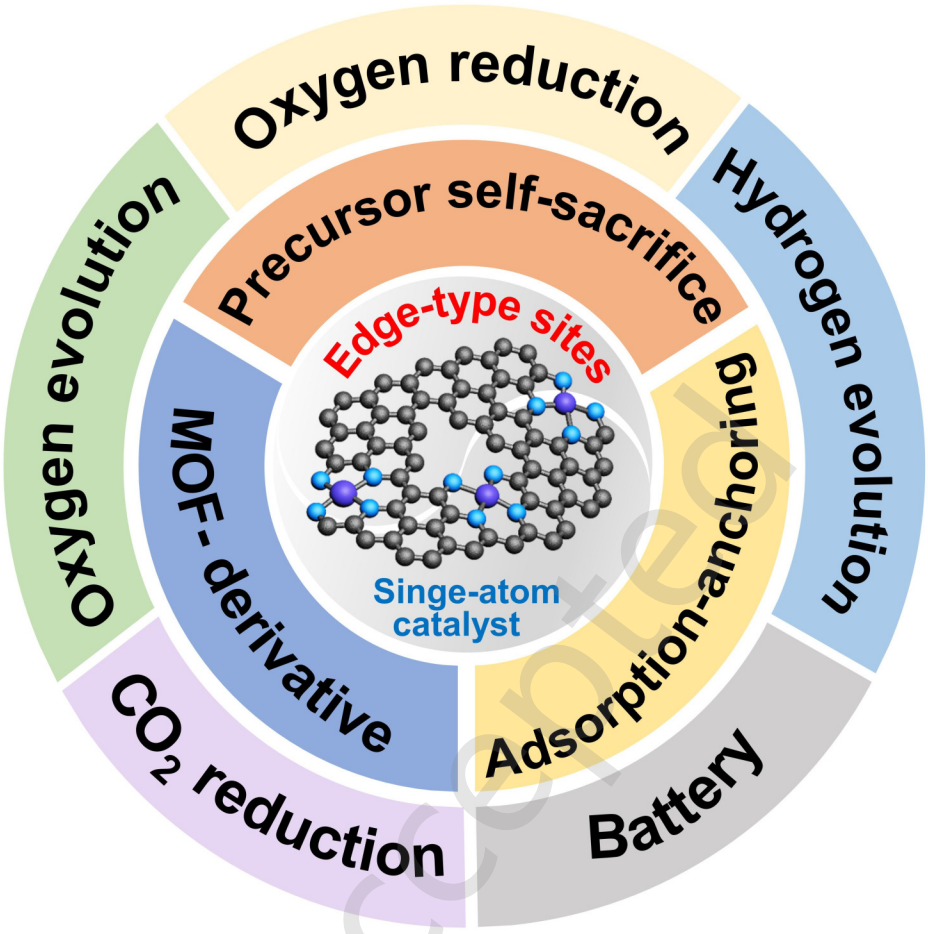

This review systematically summarized the preparation methods of edge-type single-atom catalysts and their electrocatalytic applications, focusing on how edge structures boost catalytic activity and expand single-atom catalysts use in energy conversion.

Nano Research

Open Access

Research Article

Edge-rich carbon-based single-atom catalysts: Recent progress and critical contributions to electrocatalytic applications

Chenghong Hu, Yuwei Wang, Hafiz Muhammad Adeel Sharif, Yang Cai, Linxiao Hou, Xuelei Yan, and Changping Li

Research Center for Eco-Environmental Engineering, Dongguan University of Technology, Dongguan 523808, China

Received: 19 March 2026; **Revised:** 8 May 2026; **Accepted:** 12 May 2026

Address correspondence to licpbit@hotmail.com

Cite this article: *Nano Research*, 2026, 19, 94908835 https://doi.org/10.26599/NR.2026.94908835

ABSTRACT: Amid the global push for energy transition and carbon neutrality, constructing highly active electrocatalysts is essential to overcome the challenges of energy conversion and storage. N-doped carbon substrate-based single-atom catalysts (SA/NCs), with a clear reaction center, robust stability, and excellent electrical conductivity, have emerged as a key focus in electrocatalytic research. However, traditional SA/NCs mainly exhibit a porphyrin-like planar M–N_4 configuration, with a symmetrical charge distribution that limits their catalytic efficiency. Recently, the development of edge-rich NC substrates to anchor edge-type metal sites (eSA/NCs) can induce charge rearrangement and promote the exposure of active sites, leading to significantly enhanced electrocatalytic performance. This review provides a comprehensive summary of eSA/NCs for electrocatalytic reactions. First, the synthetic strategies of eSA/NCs are classified, and the main characterization techniques are introduced. Subsequently, the performance of eSA/NCs in diverse electrocatalytic reactions is carefully discussed, with emphasis on elucidating the structure-activity relationships underpinned by edge structure. Finally, regarding the issues of controllable construction and quantitative analysis of the current NC substrates with high edge density, we have proposed feasible development directions and strategies. This work highlights the significance of edge structure contributions in enhancing the catalytic efficiency of SA/NCs and provides technical guidance for designing future high-performance electrocatalysts.

KEYWORDS: single-atom catalyst, N-doped carbon substrate, edge structure, synthetic strategy, electrocatalytic applications, structure-function relationship

1. Introduction

With rapid population growth and industrial expansion, the excessive exploitation and inefficient utilization of fossil fuels have accelerated the depletion of non-renewable resources and the emission of greenhouse gases, leading to serious energy crises and environmental pollution problems [1, 2]. Consequently, the exploration of renewable energy conversion technologies to mitigate global energy and environmental challenges stands at the forefront of current research. Electrocatalytic technology has emerged as a strong candidate for sustainable energy conversion, as it can be driven by green energy set-up (such as wind, solar, tidal energy, etc.) and catalytically convert energy-related small molecules into value-added chemicals and clean fuels through controllable electrochemical reactions [3-8]. Electrocatalytic reactions predominantly occur on the interface of heterogeneous catalysts, which involves the initial reactant adsorption, followed by activation, continuous intermediate conversion, and the final desorption from active sites to obtain the target product. The slow kinetics and complex reaction pathways brought significant obstacles to the practical applications [9, 10]. The efficient electrocatalysts exhibited a key role to improve the efficiency of these reactions [11, 12]. At present, precious metal catalysts show the highest activity in electrocatalytic research, but their shortage stock and expensive price characters limit their wide application [13-19]. Thus, in the face of the huge demand for electrocatalytic applications, exploring efficient and low-cost catalysts has become the focus of attention for researchers around the world.

The construction of single-atom catalysts (SACs) by dispersing metal atoms as isolated sites on substrates has emerged as a highly dynamic research object in energy-related catalytic conversion research [20-23]. SACs exhibit near-100% efficiency of atomic utilization, distinct active centers, and tunable electronic structures, offering a promising solution to the challenges of excessive metal consumption and high fabrication costs associated with conventional catalyst [23-25]. The research on SACs has been continuously updated and expanded in various directions, from carrier design (such as metal/metallic compound, porous organic polymers, and carbon-based substrates, etc.) to coordination environment regulation (coordination atoms types, quantities, distances, etc.) [26-28]. Among these, N-doped carbon substrate-based SACs (SA/NCs), owing to their exceptional conductivity, morphologically controllable architectures, and chemically tailorable compositions, have demonstrated broad applicability across diverse electrocatalytic processes [29-32].

Through in-depth research, the limitations of SA/NCs have been identified as arising from the coordination form and substrate structure. Firstly, the metal sites in SA/NCs predominantly adopt the M–N_4 coordination configuration, with highly symmetrical charge distribution leading to a relatively high reaction energy barrier for substrate adsorption and activation as well as for intermediate transformation [33-37]. Secondly, the dense carbon substrate impedes the accessibility of active sites, making it difficult for the reactive material to penetrate and contact the active center, and the reaction products cannot diffuse into the external electrolyte in time [38-41]. Based on the above problems, two key solution have been proposed to boost the catalytic efficiency of SA/NCs: one approach involves optimizing the metal coordination environment to modulate electronic structure, thereby reducing energy barriers, and the other is to enhance the accessibility of metal sites through morphology modification of the carbon substrate (Figure 1) [42-50]. However, for the highly stable M–N_4 configuration, the regulatory effect of heterogeneous atom doping is limited, and the disordered hierarchical pore structure can only release a small number of active sites, causing the improvement in SA/NCs activity is not obvious. The means to achieve effective electronic structure optimization and maximize the accessibility of active sites simultaneously still need further exploration.

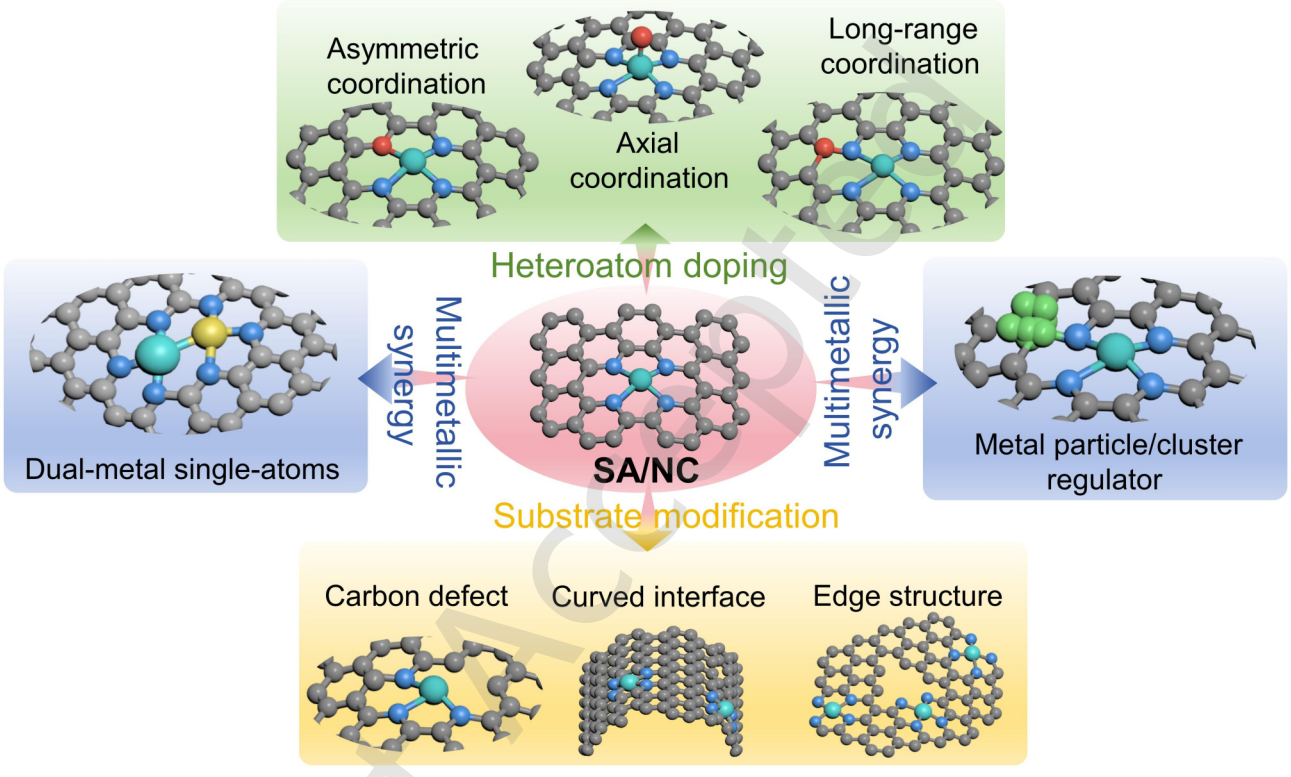

Figure 1. Regulatory strategies for the catalytic activity of SA/NCs.

Recently, using edge-rich NC substrates to anchor metal sites and obtain edge-type single-atom catalysts (eSA/NCs) has become a burgeoning research focus in electrocatalysis [51, 52]. Compared to in-plane M–N_4 sites, edge-hosted M–N_4 sites exhibit superior catalytic performance, attributable to their dangling bonds at sp^2-hybridized carbon edges, which induce localized electronic redistribution and modulate the bonding environment around metal sites [53-55]. The special edge structure enhances SA/NCs catalytic activity by optimizing electronic structures and synergistically exposing active sites. This work presents the first comprehensive review of the design strategies and electrocatalytic applications of edge-rich carbon-based eSA/NCs, elucidating the mechanistic role of edge-structure in catalytic enhancement (Figure 2).

First, we systematically categorize state-of-the-art fabrication approaches for edge structure design to anchor metal sites. Subsequently, we critically evaluate eSA/NCs applications in oxygen evolution reaction (OER), hydrogen evolution reaction (HER), oxygen reduction reaction (ORR), CO_2 reduction reaction (CO_2RR), and battery energy storage technologies. Through the synergistic integration of experimental data and density functional theory (DFT) calculations, this review provides a detailed elaboration on how edge structure engineering regulates the electronic structure and morphology of SA/NCs, while also clarifying the underlying effect mechanism of the edge structure on the activity and reaction pathway of SA/NCs. Finally, by summarizing the latest research on the application and mechanism of eSA/NCs, this study identifies key challenges and proposes future development directions, thereby providing a theoretical foundation and experimental basis for the innovation of high-activity eSA/NCs.

2. Edge-structure engineering for the construction of eSA/NCs

Substrate material selection critically determines the coordination environment and catalytic activity of single-atom metal sites. Current synthetic methodologies enable the precise anchoring of individual metal atoms on diverse substrates, including metals/metal oxides, carbonaceous materials, organic polymers, and others [56-58]. For

electrocatalytic applications, NC substrates are the optimal choice due to their excellent electrical conductivity, structural durability, and catalytic inertness. To enhance the activity of SA/NCs, multifaceted strategies have been developed: (1) Morphological optimization of carbon substrates (e.g., geometric configuration engineering, defect implantation, pore size modulation, edge structure enrichment). (2) Chemical composition modulation (e.g., light heteroatom doping, secondary metal sites incorporation). (3) Coordination environment engineering (e.g., heteroatomic types, coordination numbers, and bond distances) [59-61]. Among these, edge structure engineering stands out as a pivotal factor for enhancing active site performance, conferring the advantages of easily broken charge distribution and active site accessibility compared to their in-plane counterparts [62-64]. This chapter summarizes several design strategies for eSA/NCs, providing guidance on the configuration and characterization of edge structures.

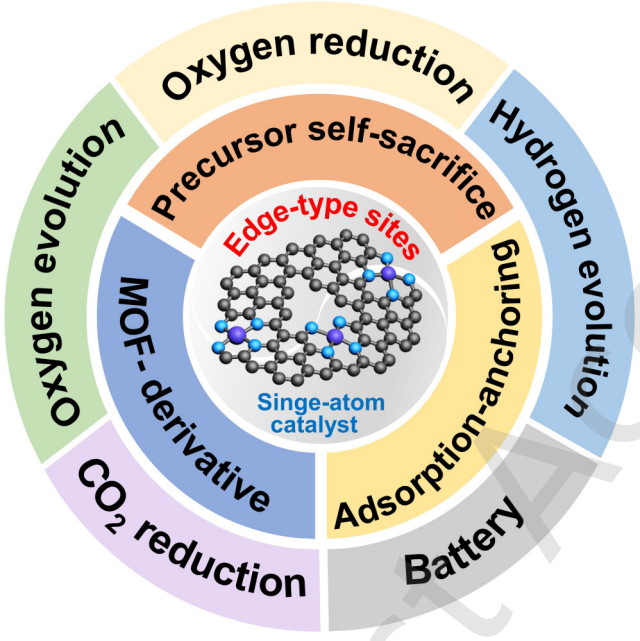

Figure 2. The main content illustration of this review.

2.1 Precursor self-sacrifice strategy

The precursor self-sacrifice method involves mixing a metal source, a carbon source, and a nitrogen source, and then obtaining single-atom metal sites anchored on rich edge structure NC substrates via high-temperature pyrolysis combined with acid-washing processes [65, 66]. This method has become an important method in the field of eSA/NCs preparation with the characteristics of simple operation and low cost.

Xiao et al. proposed a Fe-N_x-C catalyst with rich-edge substrate by adopting the precursor self-sacrifice strategy [65]. Firstly, the PDAN-Fe polymer is obtained using 1, 8-diaminaphthalene (DAN) as the monomer and $FeCl_3$ as the oxidative polymerization initiator. Then, a carbon-based materials composite with Fe clusters and Fe single atoms coexisting are obtained through pyrolysis. Finally, the acidic solution leaching method is applied to dissolve the Fe clusters close to the single-atom Fe sites, obtaining the catalyst Fe/N-G-SAC with edge FeN_x sites (Figure 3a). The pivotal advance of this work resides in the strategic utilization of an Fe-rich precursor, which engenders three synergistic advantages: (1) The Fe-rich environment facilitates the spontaneous generation of Fe atomic clusters under the high-temperature calcination process. These clusters act as catalytic centers, enhancing the graphitization of the carbonaceous substrate, thereby improving its electronic conductivity by promoting the ordered arrangement of carbon sp^2 domains. (2) The Fe clusters serve as nucleation centers for the localized deposition of FeN_4 coordination units in their vicinity. Subsequent acid etching to remove the Fe clusters leaves behind edge-terminated FeN_4 moieties with optimized electronic configurations. (3) After the removal of Fe clusters, a highly mesoporous structure forms, significantly enhancing mass transport and electron transfer, thereby improving reaction kinetics. Based on the above structural advantages, Fe/N-G-SAC exhibits excellent catalytic performance and durability for both ORR and OER, outperforming commercial precious metal catalysts (Pt/C and Ir/C).

The metal content is crucial for preparing eSA/NCs, as a composite material with coexisting particles/clusters and single-atom sites needs to be formed. Wang et al. developed a structurally controllable Fe-N_4-C catalyst and investigated the effects of metal content on porous carbon substrates and the number of edge sites [66]. Figure 3b shows the principle of edge structure and the transmission electron microscope (TEM) results of the dynamic changes in the Fe-N_4-C-x substrate (x representing the $FeCl_3$ amount) with varying initial $FeCl_3$ amounts. Clearly, when $FeCl_3$ is used at 20 mg, no Fe aggregates form on the carbon substrate after the pyrolysis. Upon increasing the $FeCl_3$ dosage to 40 mg, a single pore emerges in Fe-N_4-C-40, accompanied by a small number of edge Fe sites located at nitrogen-modified defects (e-ND−Fe) of the carbon substrate. When the $FeCl_3$ amount is increased to 60 mg, more mesoporous structures appear, indicating greater exposure of e-ND−Fe active sites. However, upon increasing the $FeCl_3$ dosage to 80 mg, the small pores coalesce into larger ones, potentially leading to partial collapse of the nanostructure and consequently reducing the number of accessible edge sites. N_2 adsorption-desorption isotherms and the pore size distribution results (Figure 3c, and 3d) show that the addition of a moderate amount of $FeCl_3$ significantly increased the number of mesopores (pore size > 2 nm). In particular, the amount of $FeCl_3$ in Fe-N_4-C-60 was the best, resulting in the largest mesoporous structure. From a geometric perspective, the two N atoms of the edge Fe-N_4 sites can only be connected to a single C atom, while the in-plane N atoms can combine with two C atoms simultaneously. Consequently, the number of more edge M–N_4 sites increases, and the content of C–N bonds decreases. As illustrated in Figure 3e, the C–N content in Fe-N_4-C-60 is the smallest, illustrating the number of edge sites in this structure is the largest. This fully demonstrates that the amount of metal source indeed plays a key step in regulating the anchoring form of metal sites.

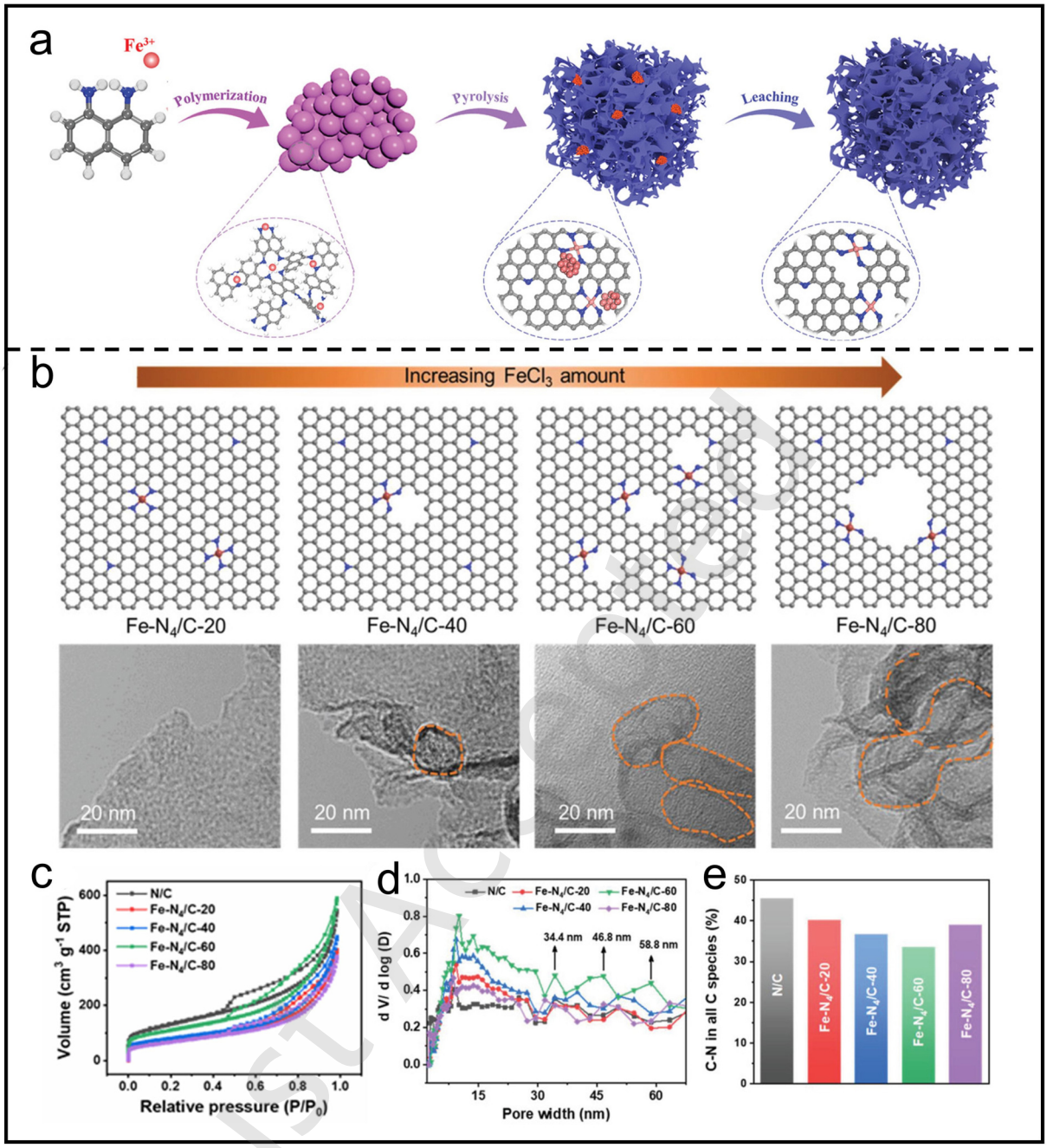

Figure 3. (a) Visual representation for the Fe/N-G-SAC synthesis. Reproduced with permission from [65]. Copyright 2020, Wiley-VCH. (b) Schematic diagrams and TEM results about the structural changes in Fe-N_4-C-x formed by using different amounts of $FeCl_3$. (c) N_2 adsorption-desorption curve, (d) pore size distribution, and (e) content ratio of C–N bonds of a series of Fe-N_4-C-x. Reproduced with permission from [66]. Copyright 2020, Wiley-VCH.

Although the self-sacrificing strategy has been extensively applied in high-performance catalyst synthesis, the morphology of the carbon substrate derived from it is difficult to control. The generation of internal mesoporous depends on the pre-occupying effect of metal particles or clusters, and the proportion of single-atom sites at the edges is low. Furthermore, the disordered distribution of micro and meso-pores leads to limited internal mass transfer, and the accessibility of high-performance edge metal sites is insufficient. Therefore, this process should continue to be upgraded and optimized, such as in combination with the hard template method or the precursor self-assembly technology structure, to construct edge-rich carbon substrate with ordered porous structures.

2.2. MOFs derivative strategy

Metal-organic frameworks (MOFs) are porous material by the self-assembly of metal species and organic ligands, featuring high porosity, high surface area, and easy functionalization [67-69]. The periodic arrangement characteristic of MOFs structure makes them excellent precursors for the design of metal single-site anchored carriers [70]. Especially, the N-rich zeolitic-imidazolate framework (ZIF-8) is widely used in the manufacture of eSA/NCs [71-74]. The method for preparing eSA/NCs using the ZIF-8 precursor mainly involves high-temperature pyrolysis without disrupting the ordered porous structure and framework morphology of the precursor, and the formation of mesoporous carbon defects or hierarchical pore

structures within it, leading to single-atom metal sites located at carbon substrate edges.

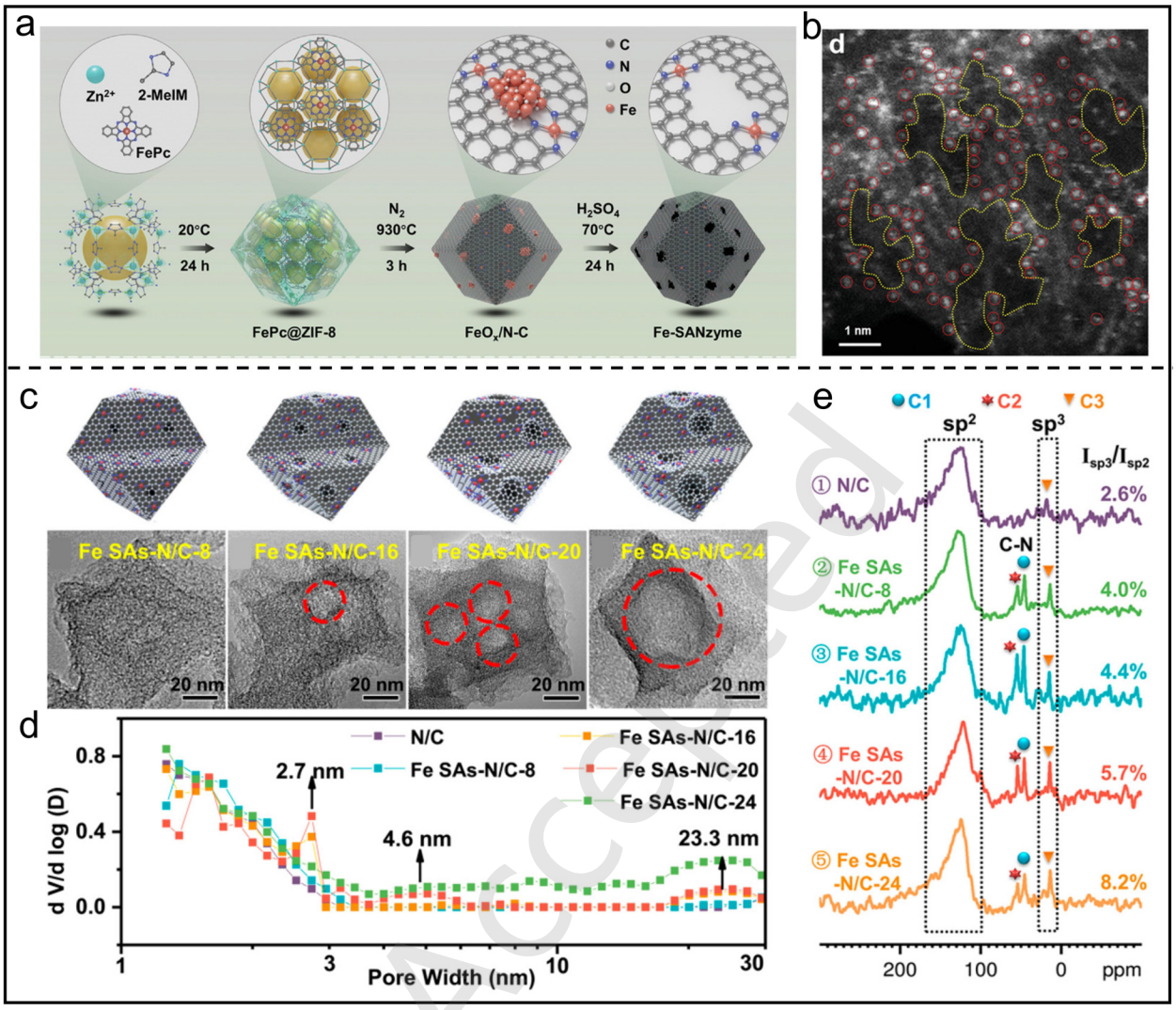

Figure 4. (a) Schematic process for Fe-SANzyme based ZIF-8 synthesis. (b) AC HAADF-STEM result of Fe-SANzyme. Reproduced with permission from [75]. Copyright 2022, Wiley-VCH. (c) Schematic and TEM images, (d) Pore size distribution, and (e) ^{13}C-ssNMR spectra of Fe SAs-N/C-x derives from ZIF-8 precursor with different amounts of FePc. Reproduced with permission from [77]. Copyright 2018, American Chemical Society.

Based on the different ways of forming edge structures, the main preparation methods of ZIF-8 derived eSA/NCs are divided into two categories. One is a self-assembly method for encapsulating metal objects. First, during the preparation of ZIF-8, the metal source is introduced and fixed within the pores. Then, high-temperature pyrolysis was applied to obtain the carbon-based composite material with coexisting particles and single-atom sites. By leveraging the acid instability of metal particles, they are selectively stripped away with an acidic solution, enabling the formation of edge single-atom sites. For instance, Zhang et al. prepared an eSA/NCs with defect carbon-loaded Fe-N_4 sites through edge-structure engineering using ZIF-8 as the medium (Figure 4a) [75]. First, Fe phthalocyanine (FePc) molecules (metal and N double precursors) are loaded into the cavity of ZIF-8 through a one-pot method to prepare FePc@ZIF-8 composites. Since the diameter of FePc (14.6 Å) is greater than the cavity size of ZIF-8 (11.6 Å), the constraint effect of the cavity is broken, promoting the rupture of the cavity. Subsequently, an NC substrate loaded with Fe species is synthesized via high-temperature pyrolysis. During this process, FePc embedded in the fractured cavity was in-situ reduced to an Fe/N precursor, forming mesoporous Fe-N_x sites. In addition, the additional FePc multi-molecular aggregates are induced to form FeO_x nanoclusters through the Kirkendall effect, thereby further enriching and expanding mesoporous defects [76]. The final hierarchical porous Fe-SANzyme was prepared after removing the excess metals in the hybridized FeO_x/N-C nanocomposites by acid leaching. The images of aberration-corrected high-angle annular dark field STEM (AC HAADF-STEM) display that the dispersive Fe atoms are homogeneously located in the main body and defect edges of the hierarchical porous carbon matrix, confirming that this strategy successfully transformed some metal single atoms from in-plane to edge configuration transformation (Figure 4b). Although this study presents a method for synthesizing eSA/NCs from ZIF-8, it fails to deeply investigate the intrinsic relationship among FePc content, edge structure formation, and edge site density. Nor does it provide sufficient robust characterization to verify the formation of edge sites.

By adjusting the amount of FePc in the self-assembly

process, the defect content and the number of edge sites inside the eSA/NCs can be regulated. Jiang et al. developed a method to immobilize the atomically dispersed Fe-N_4 on the hierarchical porous carbon substrate through controlling the addition amount of FePc during the synthesis of ZIF-8, and precisely characterized the constitution principle of C–N defects [77]. The mechanism diagram and TEM images demonstrate that with increasing FePc content, inner cavities form within the carbon substrate and gradually expand (Figure 4c). The pore size distribution proved the formation of hierarchical meso-microporous structures within Fe SAs-N/C-x (Figure 4d). To further prove that the formation of internal mesopores and the increase of pore size may induce the fracture of C–N bonds. The author developed a detailed research on the chemical bond network of porous carbon substrate by using ^{13}C solid-state nuclear magnetic resonance (ssNMR). The spectrum of the original N/C material exhibits a broad peak at δ = 100–170 ppm, which is attributed to the signal of the graphite-like sp^2-hybridized carbon structure (Figure 4e). Further, the signals of N-alkyl carbon began to appear in Fe SAs-N/C-x (C1 at 45.6 ppm and C2 at 53.9 ppm), which is caused by the disruption of the C=N bond in graphite N and pyridine N. With the increase of FePc content, the C1 and C2 signals are further enhanced, confirming that the precise splitting of the C–N bond exists over the pore size expanding process. Therefore, the pore engineering based on ZIF-8 can induce C–N bond splitting near the metal sites and promote the formation of edge M–N_4 sites.

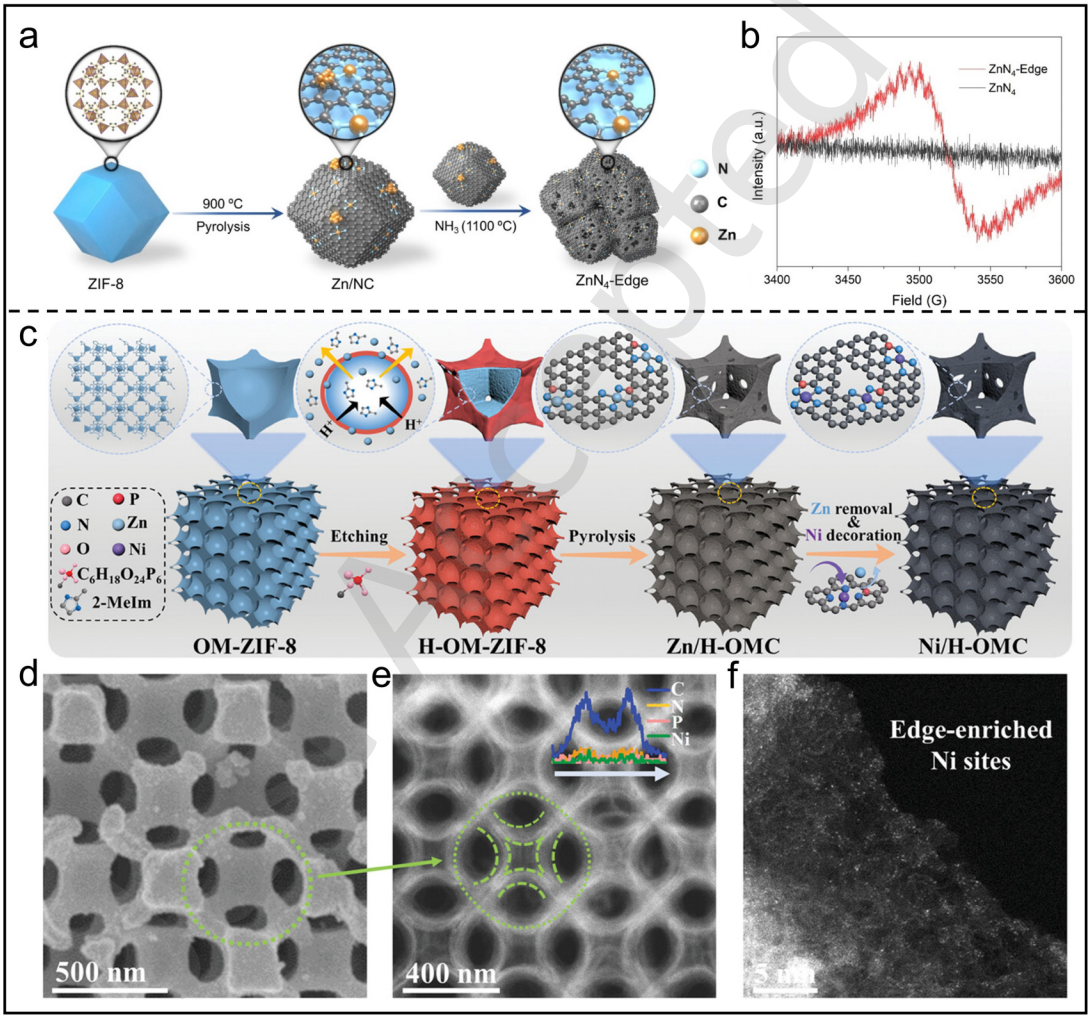

Figure 5. (a) Preparation route of ZnN_4-Edge based on ZIF-8 precursor. (b) EPR spectra of ZnN_4 and ZnN_4-Edge composites. Reproduced with permission from [81]. Copyright 2023, National Academy of Sciences. (c) Schematic representation of the Ni/H-OMC synthesis. (d) SEM, and (e) HAADF-STEM results of Ni/H-OMC. (f) AC HAADF-STEM image of Ni/H-OMC. Reproduced with permission from [86]. Copyright 2024, Wiley-VCH.

Another method for preparing eSA/NCs using ZIF-8 precursors is the gas or liquid phase etching method. Based on the acid and alkali intolerance of the ZIF-8 structure, it can be etched by acidic/alkaline gases or organic solvents to promote the partial dissociation of the metal from the ligand and construct hierarchical porous and/or hollow structures of carbon substrate, thereby increasing the proportion of the edges [78, 79]. For the gas-phase etching method, this process is generally completed during the high-temperature calcination process. For example, Kong et al. used acetate as the etching gas to optimize the pore size of ZIF-8 [80]. The evaporation of acidic gases promotes the disengagement of metal from ligands, resulting in the generation of a hierarchical carbon nanocage structure. For the ORR performance test, edge structure exhibits higher accessibility of metal active sites and enhances mass transfer capacity than the unetched material, which shows extremely high

half-wave potential ($E_{1/2}$) values of 0.94 V and 0.82 V, respectively. Similarly, alkaline gases can also be utilized to construct mesoporous structures within ZIF-8 and promote the expression of edges. Yu et al. proposed a two-step ways to prepare a NC supported edge Zn single atoms (ZnN_4-edge) by NH_3-assisted calcination (Figure 5a) [81]. Firstly, the prepared pure ZIF-8 is heated to 900 °C under inert gas for the first pyrolysis process to form Zn NPs on the NC substrate. Then, ammonia gas is introduced, beginning the second step of pyrolysis. The introduction of NH_3 not only promotes the decomposition of Zn NPs into atomically dispersed single atomic sites, but also etches the carbon substrate to obtain a high-defect porous carbon substrate with rich edges. EPR was used to measure the electronic signals of unpaired electrons in atomic orbitals in order to assess the number of edge sites. (Figure 5b) [82, 83]. The results proved that compared with ZnN_4 prepared without NH_3, the EPR spectrum of ZnN_4-edge shows a remarkable peak at ~3500 G, which is caused by the bond breakage at the edge position. Considering the disorderly nature of mesopores generated via gas-phase etching and the potential danger of high-temperature processes, it is necessary to develop more gentle and controllable techniques for preparing edge structures.

Compared to the gas-phase etching, liquid-phase etching is safer, simpler, and the degree of etching is easier to control. A considerable number of studies have reported that using organic-acids with moderate acidity as etchants to etch and optimize the morphology of the ZIF-8 precursor can transform a microporous solid structure into a yolk-shell or hollow structure with hierarchical channels to increase the proportion of edge structures [84, 85]. Hu et al. proposed a hierarchical-ordered pore engineering based on ordered macroporous ZIF-8 materials to construct high-density edge single-atom Ni sites [86]. The ordered macroporous structure has rich edges, while the organic acid etching strategy to construct the hollow inner wall structure further increases the proportion of edge structures (Figure 5c). Unlike the gas etching method, the solvent etching method creates highly defective hollow structures instead of partial mesopores, thus enhancing the proportion of edge configurations [87, 88]. After a combination of high-temperature pyrolysis and ion exchange processes, an edge-type Ni atom catalyst Ni/H-OMC was obtained. SEM images show that Ni/H-OMC maintains an ordered macroporous structure with rich edges (Figure 5d). HAADF-STEM images show the hollow wall structure formed between the macroporous (Figure 5e), and the line scanning profile also confirms these results (inserted in Figure 5e). The AC HAADF-STEM image shows that the atomically dispersed metal single atoms are well dispersed on the ultra-thin pore walls with rich edges (Figure 5f).

The eSA/NCs derived from MOFs can inherit the high porosity and ordered pore structure of the precursors, promoting penetration of substrate and the accessibility of active sites. Furthermore, the highly adjustable chemical constituent of MOFs makes it possible to enhance the activity based on the edge metal sites. However, the current research lacks the secondary regulation of the coordination environment based on edge single-atom sites, thereby affecting the in-depth and multifunctional preparation and application. In future research, MOFs derived eSA/NCs can be taken as the basis and direction to obtain highly active electrocatalysts.

2.3. Edge-rich substrate adsorption-anchoring strategy

Carbon substrate structure and anchoring site placement govern the abundance and distribution of edge sites. Compared with the various limitations of constructing carbon defects to indirectly obtain edges through self-sacrifice and MOFs-derived strategies, the use of an edge-rich substrate for direct adsorption-anchoring of metal sites avoids the metal agglomeration, which can increase the content of metals with atomic dispersion [89, 90]. Notably, the edge structure exhibits a reduced work function and enhanced adsorption capability relative to pristine graphene, which significantly improves the number and proportion of edge sites [91, 92]. For instance, Pan et al. used mesopore-rich graphene (GO-p) to support eFe-N_4 sites, and the CO_2RR performance was significantly improved compared with the pure graphene-supported Fe-N_4 sites lacking pores (Figure 6a) [93]. The oxygen group of GO-p exhibits a strong interaction with the Fe^{3+} ion, enabling them to act as an effective host site for anchoring Fe^{3+} ions, thus forming Fe^{3+}-GO-p. Next, Fe^{3+}-GO-p is treated with urea under high-temperature nitridation, and the oxygen-containing groups on Fe^{3+}-GO-p reacted with the nitrogen-rich gases released from urea decomposition, yielding the final Fe-N-G-p catalyst. Experimental tests have confirmed that this process does not generate metal agglomerates, and the number of edge sites located Fe-N-G-p has increased by 40% compared with Fe-N-G, which has a perfect graphene structure.

Compared with the single-layer graphene sheet structure, constructing a three-dimensional flower-like structure through morphology optimization significantly enhances the proportion of edge structures. Tang et al. introduced a high proportion of asymmetric edge carbon into the Fe-N-C catalyst through morphological engineering [94]. They obtained a hierarchical porous carbon-based catalyst (FeN_4@PC) with high edge proportion and edge site number through the classical impregnation annealing method (Figure 6b). SEM and TEM images revealed the hierarchical porous shape and abundant edges of the substrate in FeN_4@PC without agglomerated metal particles (Figure 6d-f). The character of FeN_4@PC edge defect was further verified by XAFS (Figure 6c). The normalized C-K-edge XANES spectra of FeN_4@PC and FeN_4@FC (without hierarchical porous morphology) show that the intensity of C=C peaks in FeN_4@PC is significantly weaker, while that of C–H peak is stronger, indicating the presence of edge carbon defect characteristics in FeN_4@PC [95]. As a result, FeN_4@PC exhibits substantially superior catalytic activity compared to FeN_4@FC. The above results confirm that the 3D flower-like structure has a higher edge occupancy rate than single-layer graphene carbon, and can be used to anchor a greater number of edge sites.

The use of edge-rich carbon substrate avoids the defect of metal agglomeration and increases the utilization efficiency of metal atoms. Theoretically, an adequate number of adsorption sites ensures that the quantity of edge sites is not constrained by an upper bound. However, existing edge-rich

carbon substrates, including graphene sheets, flower-like structures, etc., have a relatively low proportion of their edge structures, resulting in a limited number of metal atoms adsorbed and anchored by them. Combining edge-rich substrate with etching strategies to transform solid structures into hollow or hierarchical porous forms can further increase the proportion of edge structures.

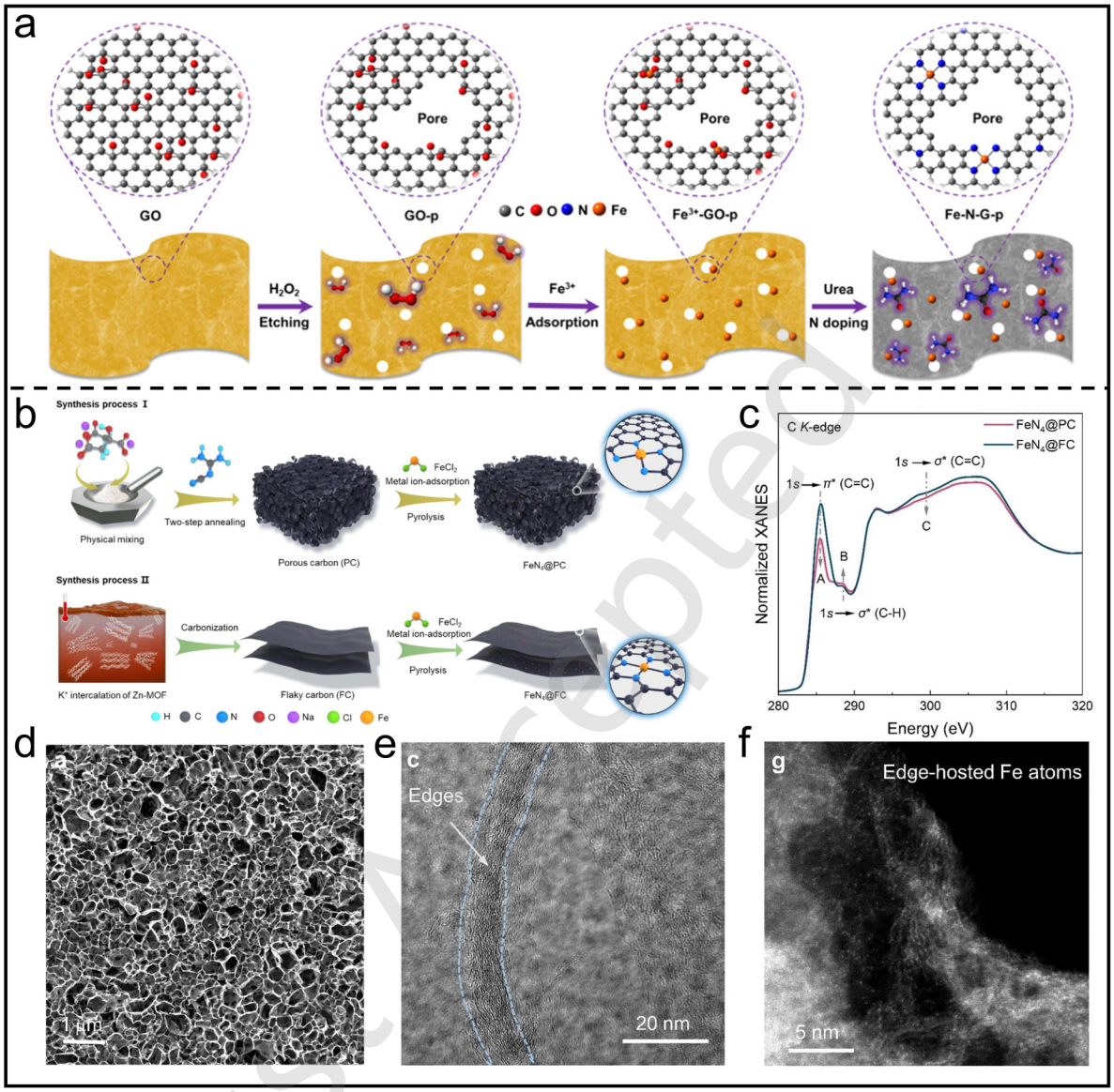

Figure 6. (a) Graphical representation for Fe-N-G-p synthesis. Reproduced with permission from [93]. Copyright 2020, American Chemical Society. (b) Preparation rout for FeN_4@PC and FeN_4@FC. (c) XANES of C K-edge spectra of and FeN_4@FC. (d) SEM, (e) TEM, and (f) AC HAADF-STEM of FeN_4@PC. Reproduced with permission from [94]. Copyright 2025, Wiley-VCH.

3. eSA/NCs for various electrocatalytic applications and catalytic mechanisms

Reasonable design of carbon substrate morphology and composition for anchoring metal sites can effectively improve the performance of electrocatalytic reactions [96]. The eSA/NCs constructed through edge structure engineering exhibit unique electrocatalytic performance due to their special geometric and electronic structure characteristics. This chapter comprehensively summarizes the applications of eSA/NCs in diverse electrocatalytic reactions, including OER, HER, ORR, CO_2RR, and battery energy storage. Integrating experimental and computational approaches, the work clarifies the role of edge structures in boosting catalytic activity, particularly through charge redistribution at interfaces and regulation the energy barrier for critical intermediates.

3.1. OER

OER is a half-redox reaction that occurs on the anode side during water splitting. Due to its complex multiple-step mechanism involving proton/electron coupling, OER suffers from high thermodynamic overpotential, requiring substantial applied voltage to drive the reaction [97-99]. Ru and Ir are widely recognized as the most active OER catalysts due to their versatile redox valence states, enabling highly efficient OER catalysis at low overpotential [100, 101]. However, due to the shortage of resources and high prices, the wide application of such catalysts is limited. The ideal electrocatalyst requires a low manufacturing cost and relatively fast kinetics.

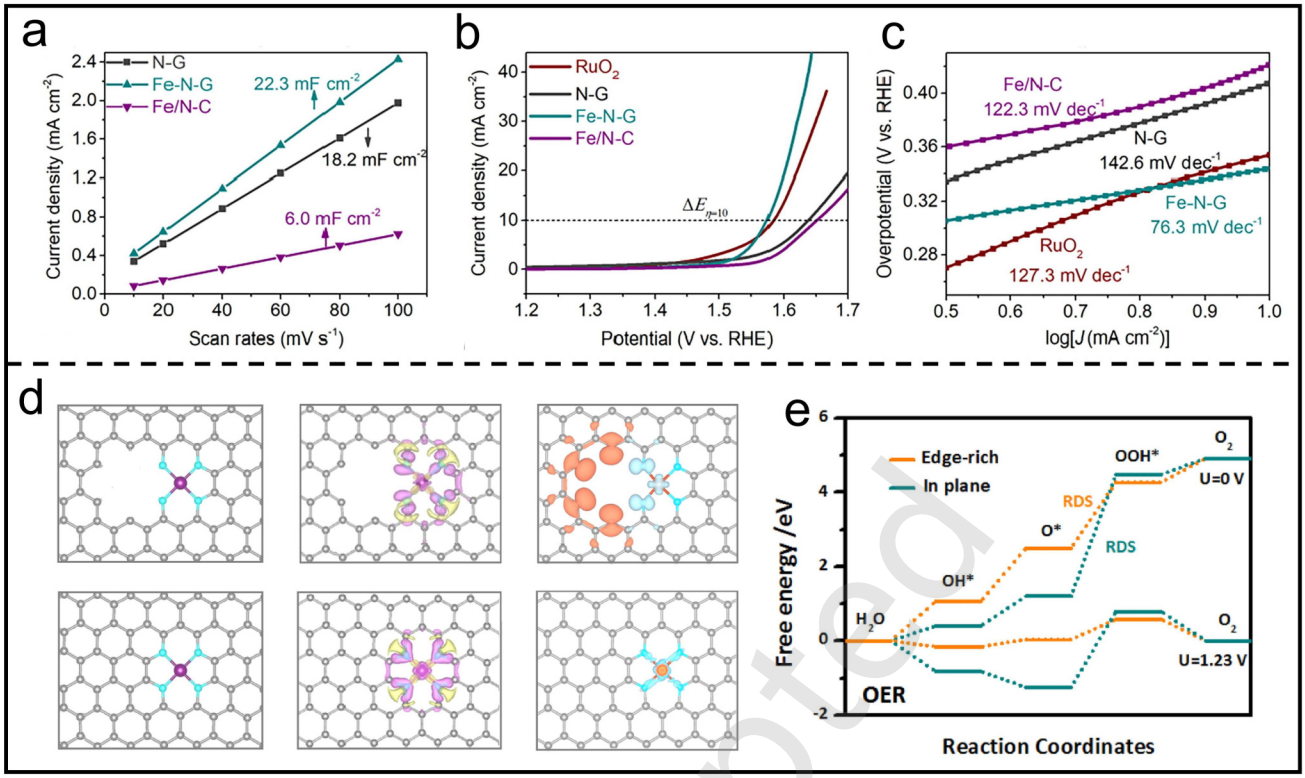

Figure 7. (a) Cdl, (b) LSV curve, and (c) tafel slope of edge-rich Fe-N-G and comparison samples. Reproduced with permission from [102]. Copyright 2023, Elsevier. (d) Atomic models, charge density differences and spin density for both edge and in-plane Ni–N_4 moieties. (e) Gibbs free energy diagrams of edge Ni–N_4 and in-plane Ni-N_4 models in the OER. Reproduced with permission from [64]. Copyright 2022, Elsevier.

The special electronic structure of edge single-atom sites endows eSA/NCs with excellent OER activity. For example, Gan et al. produced a silica-assisted method that integrates readily available edge Fe-N_x sites into porous graphite carbon (referred to as Fe-N-G) [102]. The electrochemical active surface area (ECSA) was evaluated via double-layer capacitance (C_{dl}) measurements. Fe-N-G exhibits a significantly higher C_{dl} value (22.3 mF cm^{-2}) than the in-plane Fe site catalyst Fe/N-C (6.0 mF cm^{-2}), as shown in Figure 7a. The LSV curves show that the overpotential of Fe-N-G at 10 mA cm^{-2} is 344 mV, which is obviously lower than that of Fe/N-C (422 mV) and decreased by 10 mV compared with the traditional commercial noble metal catalyst RuO_2 (Figure 7b). Notably, Fe-N-G exhibits the lowest tafel slope (76.3 mV dec^{-1}), outperforming Fe/N-C (122.3 mV dec^{-1}) and RuO2 (127.3 mV dec^{-1}) (Figure 7c). The above results proved that the engineering of edge sites markedly improves the OER kinetics and active sites accessibility.

To understand the infection regularity of the geometric anchoring environment of eSA/NCs on their electronic structure and OER performance, Zhou et al. constructed a defect-rich carbon nanotube-supported edge Ni–N_4 catalyst (Ni/N-ESC). They conducted in-depth research by combining experiments and theoretical calculations [64]. DFT calculation was used as the theoretical exploration of OER activity. The charge density difference maps clearly demonstrate pronounced electron delocalization in both edge-type and in-plane Ni–N_4 configurations, revealing substantial charge transfer from Ni centers to their coordinated N atoms and confirming their strong electronic interactions (Figures 7d). The edge Ni–N_4 sites demonstrate significant electronic redistribution and structural asymmetry compared to the in-plane sites. In addition, compared with the in-plane Ni–N_4 sites, obvious spin polarization is detected at the edge position, with more unpaired electrons, which is beneficial for reactant adsorption [103, 104]. The calculated free energy barriers of each model at 0 V and 1.23 V during OER operation reveal that the formation of OOH* exhibits the most significant free energy barrier difference, identifying this step as the rate-determining step (ΔG_{RDS}) (Figure 7e). The ΔG_{RDS} value of the edge Ni–N_4 site is significantly lower than that of the in-plane sites, verifying that the edge sites have better OER performance. The performance comparison of OER shows that Ni/N-ESC has superior catalytic activity compared to traditional SA/NCs.

The above studies reveal that the superior catalytic performance of edge sites in the OER reaction stems from their ability to disrupt charge symmetry distribution at M–N_4 sites while promoting surface charge transfer. Notably, the edge sites exhibit stronger spin polarization intensity compared to their in-plane counterparts, resulting in a greater abundance of unpaired electrons. The edge-structured sites promote the adsorption/desorption behavior kinetics of reaction intermediates and lower the energy barrier of the RDS, leading to enhanced overall OER catalytic efficiency. However, the instability of the carbon substrate under oxidative potentials still restricts the in-depth application of eSA/NCs in the OER, with most relevant studies thus focusing on electroreduction reactions instead.

Table 1. The performance comparison of Ni/N-ESC and recent SA/NCs for the OER.

Catalyst	Overpetential (j = 10 mA cm^{-1})	Tafel slope (mV dec^{-1})	Stability	Reference
Ni/N-ESC hollow fiber	293	46.7	20 h	[64]
Fe/N-G-SAC	370	73.0	2000 cycle	[65]
Ni-N_4/GHS	400	86.0	10000 s	[105]
Ni@N-HCGHF	260	63	10 h	[106]
Co_4N@NC	290	67.9	10000 s	[107]
CoNi-SAs/NC	340	58.7	10 h	[108]
CoN-HPCNF-900	400	135	/	[109]
3D Co/N-C	330	51	10 h	[110]
SS-Co-SAC	348	94.2	10000 s	[111]
MnCoNi-C-D	368	77.3	10000 s	[112]

3.2. HER

HER serves as the cathodic half-reaction in electrochemical water-splitting [113, 114], has emerged as a leading H_2 production technology due to its flexibility and carbon-free process. Although the HER process is very simple, it is still a multi-step chemical reaction, including three steps on the electrode surface: adsorption, reduction and desorption. Research has found that the local electric field generated by electron aggregation can accelerate catalytic kinetics [115]. Therefore, by designing and adjusting the local structure of the active sites of single-atoms metal site to enhance the adsorption of H_2O and achieve the enhancement of the electric field, the HER activity can be effectively improved.

Zhang et al. constructed an efficient eSA/NC by anchoring Ru atoms in polydopamine (PDA) particles with rich edge morphology (ECM@Ru) (Figure 8a) [116]. XAFS data confirmed that Ru is anchored to carbon support in an atomically dispersed atom coordination with N, and the Ru–N bond in ECM@Ru is shorter in the R-space compared to the edge-free carbon-supported Ru SA/NC (CM@Ru), confirming the difference in their coordination environment (Figure 8b). LSV analysis shows ECM@Ru achieves an onset potential close to 0 V, with overpotentials of 63 mV and 102 mV for 10 mA cm^{-2} and 50 mA cm^{-2}, respectively. This performance surpasses CM@Ru and rivals that of commercial Pt/C-20% (Figure 8c). The tafel slope of ECM@Ru is 47 mV dec^{-1}, while the tafel slopes of Pt/C-20% and CM@Ru are 29 and 76 mV dec^{-1}, respectively, demonstrating that the edge structure can effectively promote the dynamic process of HER (Figure 8d). The total density of states (TDOS) of the energy band structure governs electron donation and acceptance processes [117]. The partial DOS analysis exhibits that new hybrid electronic states were produced on the carbon substrate modified by Ru atoms, and the hybridization intensity of ECM@Ru was significantly higher than that of CM@Ru (Figure 8e) [118]. The interface of metals and coordinating atoms comprises the transfer of significant charges, which should be the reason for the stronger H* anchoring and higher conduction at edge sites [119]. Further, the Gibbs free energy (ΔG_{H^*}) of H* adsorption shows that ECM@Ru has the lowest ΔG_{H^*}, and the free energy barrier at the edge sites is closer to zero compared to other configurations, indicating its highest HER activity (Figure 8f) [120].

Although previous studies have demonstrated that edge structures can facilitate charge transfer, strengthen the local electric field effect, and thus boost the HER performance, H_2 generation fundamentally requires the coupling of H* intermediates at adjacent metal sites. Owing to the relatively dispersed nature of single-atom sites in eSA/NCs, their HER activity remains inferior to that of metal nanoparticles. Accordingly, future research should focus on increasing metal site density and constructing bimetallic sites to increase the coupling of H*.

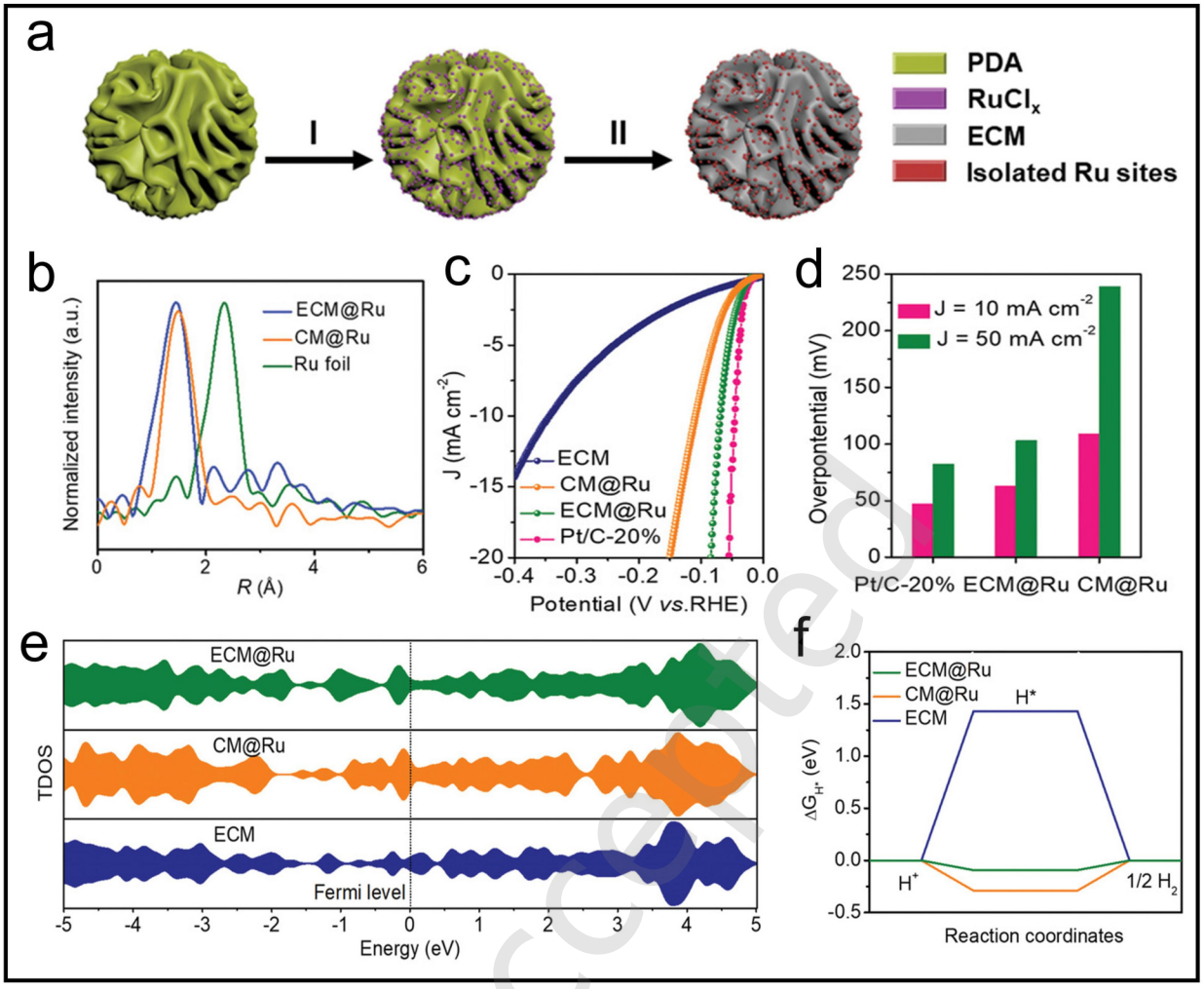

Figure 8. (a) Preparation of ECM@Ru. (b) EXAFS spectra of Ru K-edge in R space. (c) LSV curve and (d) tafel slop of various catalysts. (e) Calculated TDOS, and (f) ΔG_{H^*} on various catalysts. Reproduced with permission from [116]. Copyright 2020, Wiley-VCH.

3.3. ORR

ORR serves as a cornerstone in renewable energy technologies, functioning as a pivotal process in fuel cells and metal-air batteries [121-123]. ORR is a gaseous reduction process, in which O_2 molecules are transformed into OH^- and H_2O through a four-proton-coupled electron transfer pathway [124]. In the actual catalytic process, ORR always undergoes complex dynamic evolution, and the accompanying reaction intermediates and final products also undergo continuous transformation and reformation [125, 126]. The rational design and mechanistic analysis of catalytic materials featuring well-defined active sites and high intrinsic activity are critical for optimizing reaction kinetics, leading to enhanced performance in energy storage devices, including fuel cells and metal-air.

Tuning the binding affinity of oxygen intermediates (e.g., *OOH) to metal sites is a validated approach to boost ORR activity [54, 127]. The asymmetric charge distribution at the edge and the adjacent carbon defects with electron-induced effects jointly affect the electronic structure and properties of the metal active site microenvironment, which can balance the generation of *OOH and the reduction of *OH intermediates, thus, enhancing the catalyst performance during ORR. Tang et al. prepared the edge-type FeN_4 sites catalyst (FeN_4/PC) using an adsorption-anchoring strategy on an edge-rich hierarchical porous carbon substrate with a half-wave potential ($E_{1/2}$) of 0.809 V, which is superior to the planar metal-sites catalyst FeN_4@FC (0.737 V) and comparable to the commercial Pt/C catalyst of 0.813 V (Figure 9a) [94]. The charge density differences between the edge FeN_4 site and the in-plane FeN_4 site are presented in Figure 9b and 9c. Compared with the charge symmetrically distributed in-plane site, the asymmetric geometric structure of edge FeN_4 leads to charge reconstruction and the non-uniform distribution around the Fe sites. The lower local electron density is conducive to the electron transfer of Fe sites, which is beneficial for the adsorption and reduction of O at the edge FeN_4 sites, thereby improving the ORR activity [128, 129].

Interestingly, the metal-substrate interaction not only governs the activity of the metal sites, but the effect of edge structure can also be used to modulate the reaction pathway of ORR. For instance, Tian et al. reported the use of the edge effect of carbon substrate to regulate the ORR route on Co-SACs [130]. The correlation between the reaction energy of ORR and the local geometric shape of the anchor point was theoretically studied by using DFT analysis. Based on the binding locations at the defect sites of solo-layer graphene, five types of Co–N_4 configurations were created (Figure 9d). The formation energy of Co–N_4 arrangements was evaluated

by calculating the energy change upon Co atom embedding into the N-doped graphene matrix (Figure 9e). For 2e⁻ ORR, the catalytic efficiency is governed by the O_2 activation pathway and the OOH* desorption step, which are critical to the overall reaction kinetics. Therefore, the free energy of adsorption for OOH* (ΔG_{OOH^*}) is usable as a main parameter for predicting the reactivity [131]. Theoretically, in the ORR process of 2e⁻, ΔG_{OOH^*} should be approximately 4.2 eV, and thus the thermodynamic potential (U_L) is near the equilibrium potential of 0.7 V, and the overpotential is the smallest [132]. While the ORR process of 4e⁻, the optimal ΔG_{OOH^*} should be ~3.9 eV [133]. The active volcano map (Figure 9f) was constructed as a function of ΔG_{OOH^*} based on the calculation results. Co-N_4/G resides on the left leg of the volcano plot (ΔG_{OOH^*} = 3.93 eV), where strong *OOH binding promotes the 4e⁻ ORR pathway. Conversely, when Co–N_4 exists in the defective pockets and edge positions, the binding strength of *OOH weakens [134]. These results indicate that the position of the anchoring sites influences the ORR energy barrier, and the Co–N_4 sites carried at the edge are advantageous for 2e⁻ ORR than those carried on the base plane.

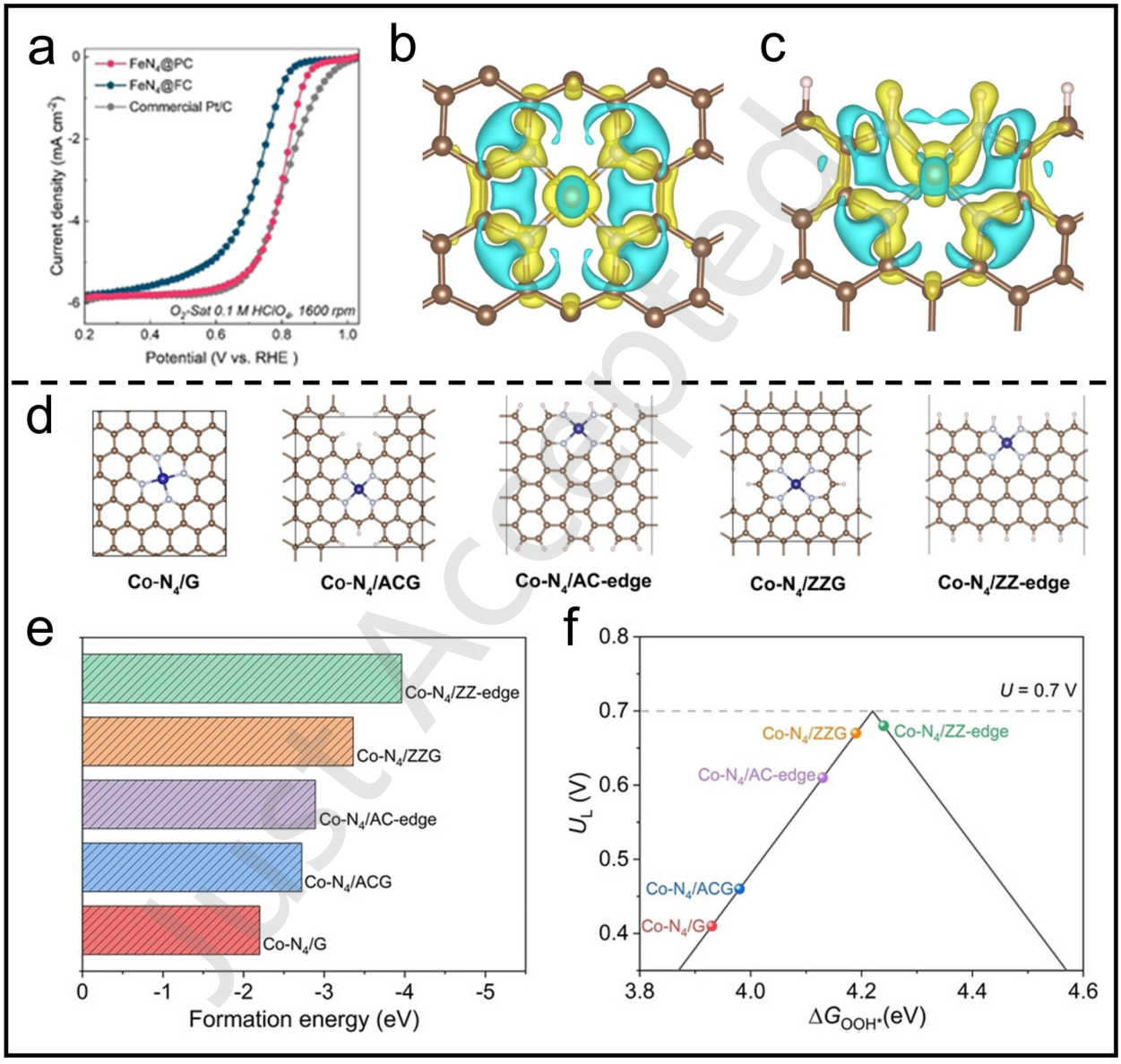

Figure 9. (a) ORR polarization curves of FeN_4@PC, FeN_4@FC and commercial Pt/C. (b) Charge density difference of FeN_4 site in plane and (c) edge. Reproduced with permission from [94]. Copyright 2025, Wiley-VCH. (d) The optimized structural models, (e) calculated formation energies and (f) volcano plot for 2e⁻-ORR of different Co–N–C structures. Reproduced with permission from [130]. Copyright 2022, Wiley-VCH.

Table 2 displays a comparison of the ORR performance between eSA/NCs represented by FeSA-N/Cs-OAc, eFe-N_3/PCF and the traditional SA/NCs, fully demonstrating the outstanding performance of the edge sites in terms of ORR. The edge geometry modulates the valence state and charge distribution of the metal center, inducing asymmetric charge distribution at edge sites to optimize the reaction energy of key ORR intermediates. The enhanced metal-substrate interaction also promotes the electron transfer on the surface and enhances the reaction kinetics. The edge structure provides a new development direction for the local geometric design and precise regulation of the electronic structure of ORR catalysts.

Table 2. The performance comparison of eSA/NCs and reported SA/NCs for the ORR.

Catalyst	Electrolyte	Eonset (V)	$E_{1/2}$ (V)	Reference
FeSA-N/Cs-OAc	0.1 M KOH	1.05	0.94	[80]
eFe-N_3/PCF	0.1 M KOH	1.09	0.934	[54]
Fe-SAs/Fe_3C-Fe@NC	0.1 M KOH	0.98	0.93	[135]
Fe@NG-750	0.1 M KOH	1.03	0.90	[136]
Fe-N-C	0.1 M KOH	0.92	0.874	[137]
FeSA/B,N-CNT	0.1 M KOH	1.07	0.933	[138]
Co-SAS/HOPNC	0.1 M KOH	1.07	0.933	[139]
Fe/N,S-PC	0.1 M KOH	1.0	0.904	[140]
Fe/OES	0.1 M KOH	1.0	0.85	[141]
Fe,Mn/N-C	0.1 M KOH	0.979	0.928	[142]
FeAB-O	0.1 M KOH	0.98	0.90	[143]
Fe1-HNC-500-850	0.1 M KOH	0.93	0.842	[144]
3DOM Fe-N-C	0.1 M KOH	/	0.875	[145]
Mg-N-C	0.1 M KOH	1.04	0.91	[146]

3.4. CO_2RR

CO_2RR serves as a pivotal pathway toward carbon neutrality, enabling the conversion of CO_2 into value-added chemicals and fuels [147, 148]. Its products are widely distributed, including C_1 products such as CO and HCOOH, as well as C_{2+} products such as C_2H_4 and C_2H_5OH. At present, the SA/NCs used for CO_2 reduction are mainly transition metals, which themselves have good activity for HER. To achieve high selectivity and wide voltage window range of CO_2RR, electronic structure regulation is often required to improve the intrinsic activity of the metal sites [149-151].

The construction of edge structure has opened up a new path for enhancing the activity of the SA/NCs in CO_2RR. For instance, Liu et al. introduced Fe into Bi-MOF as a complex precursor to construct eSA/NCs [152]. By taking advantage of the low boiling point characteristic of Bi, the edge Fe sites were constructed through high-temperature evaporation of Bi species. At comparable ECSA, edge sites exhibit superior intrinsic activity to in-plane sites for CO_2RR.

With the deepening of research, acidic electrolytes are regarded as a new direction for achieving industrial density of CO_2RR due to the sufficient available H^+ and the avoidable accumulation of carbonates [153, 154]. However, the competition for HER is obvious under acidic conditions. To enhance the CO_2RR selectivity while inhibiting HER under an acid electrolyte remains a challenge. Hu et al. utilized ordered macroporous MOFs (OM-ZIF) as precursors and combined them with organic acid etching to construct edge-rich ordered macroporous and hollow wall structure carbon-supported high-density edge Ni single-atom sites (Ni/H-OMC) [86]. When the active sites of Ni-N_4/P was moved from the in-plane to the edge, the catalytic activity was significantly improved. As shown in Figures 10a and 10b, in an acidic medium, Ni/H-OMC can maintain FE_{CO} above 90% within a wide potential window of −0.9 to −1.5 V, and the current density is higher than 200 mA cm^{-2}, reaching the industrial standard. The DFT free energy barrier indicates that the construction of edge structure can further lower the reaction energy barrier on the basis of heteroatom doping regulation (Figure 10c). To clarify this enhancement effect, differential charge density and projected density of states (PDOS) were used to provide an in-depth interpretation about complex formation of the metal site and the *COOH intermediate. The results show that the introduction of the edge can significantly disrupt the charge symmetry (Figure 10d-10f) and shorten the energy band gap between the metal site and *COOH based on the traditional heteroatom doping method (Figure 10g-10i), resulting in a stronger binding of *COOH on

eNiN$_4$/P [88]. Table 3 shows a comparison of the CO_2RR performance between eSA/NCs represented by Ni/H-OMC and the traditional SA/NCs, including the maximum FE_{CO}, partial current density, the potential window of FE_{CO} > 90%, and the stabilities.

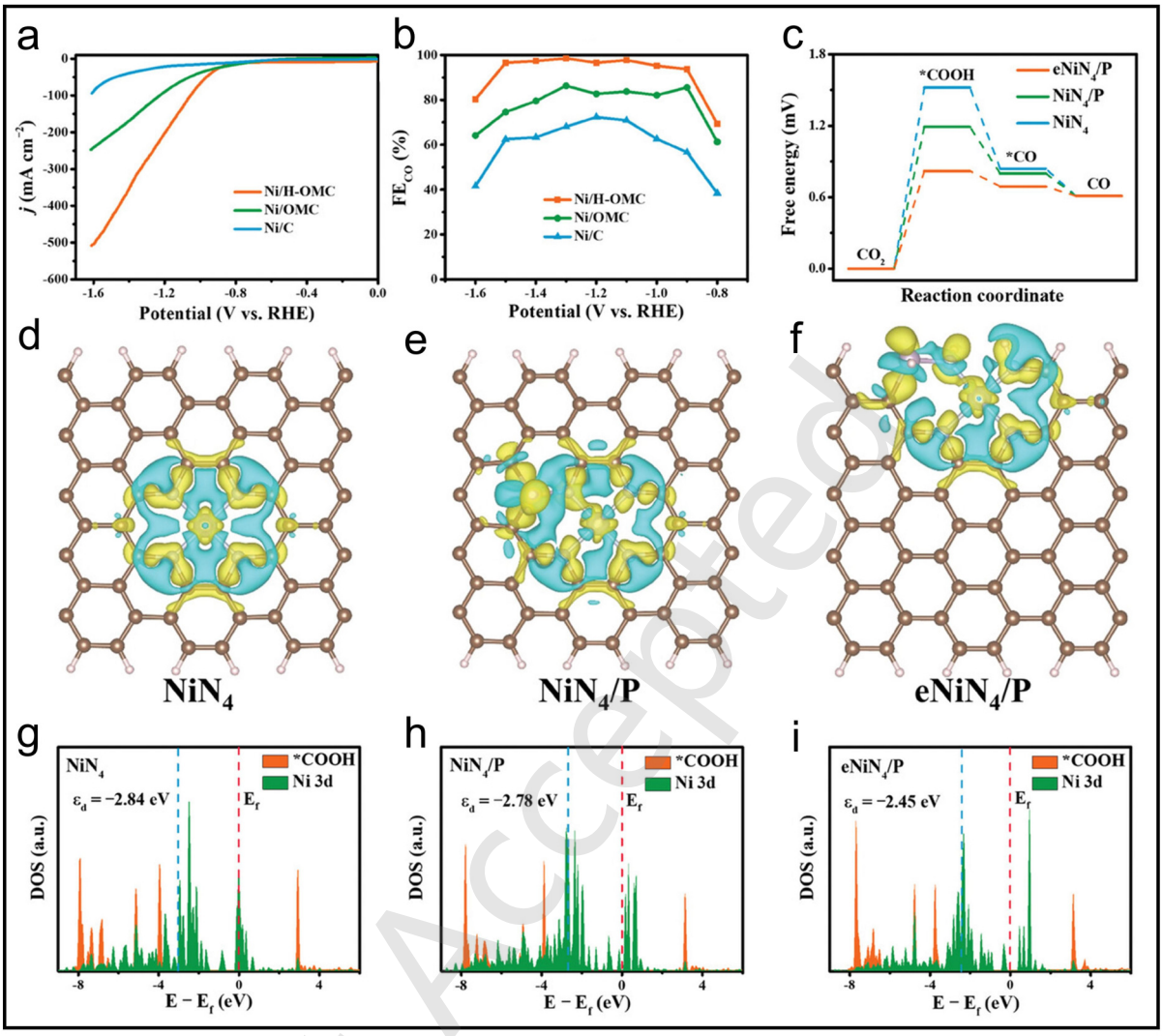

Figure 10. (a) LSV curve, and (b) FE_{CO} of different catalysts. (c) Free energy profiles, (d-e) calculated charge density differences, and (g-i) projected DOS of NiN$_4$, NiN$_4$/P, and eNiN$_4$/P models. Reproduced with permission from [86]. Copyright 2024, Wiley-VCH.

The results demonstrate that edge site construction facilitates electron configuration rearrangement, reduces the d-band center to E_f distance, and enhances intermediate adsorption, thereby exhibiting markedly higher catalytic activity than in-plane sites. However, the spatially dispersed metal atoms in eSA/NCs render it difficult to realize *CO coupling for the generation of high-value-added C_{2+} products. Therefore, increasing the density of metal sites and *CO coverage via a synthetic strategy and support structure rationally optimized, represents a key direction for the further advancement of eSA/NCs in CO_2RR applications.

3.5. Battery energy storage technology

Battery energy storage systems can provide energy for electric vehicles and offer grid-scale storage for clean and sustainable energy sources such as wind, solar, tidal and geothermal power, which is exponentially increased in the green energy field [155, 156]. With the continuous increase in the demand for fossil fuel energy, the evolution of advanced energy storage systems is of vital importance. However, problems such as low energy density, cycle instability and overpricing have restricted the development of energy storage devices. Therefore, developing advanced electrode catalysts is essential to enhance redox reactions during the charging and discharging cycles, enabling both compact energy storage and superior rate performance.

Lithium-sulfur (Li-S) batteries emerge as a leading next-generation energy storage technology, offering superior energy density and sustainability compared to conventional systems. However, their performance is limited by the shuttle effect, which arises from the accumulation of soluble lithium polysulfides (LiPSs) in the electrolyte during sulfur-related oxidation-reduction (SROR) reactions—a critical factor determining battery performance [157]. Zhang et al. proposed a polymer-induced strategy for partially anchoring FeN$_4$ to N-doped hierarchical porous carbon nanotubes to prepare a catalytic material with extremely uncovered edge Fe sites (Fe-NPC@CNTs) (Figure 11a) [158]. Figure 11b illustrates the ultrafast polysulfide conversion kinetics enabled by Fe-NPC@CNTs, which achieved an efficient "trapping-conversion" pathway mediated by edge-

distributed Fe-N_4 moieties. During discharge/charge, Fe-NPC@CNTs exhibits good chemical adsorption performance for LiPSs and also achieves fast SROR dynamics. Constant current charge-discharge curves of Li-S battery with the Fe-NPC@CNTs modified separator are shown in Figure 11c, the discharge capacity and sulfur utilization rate of the battery with Fe-NPC@CNTs modified separator are higher than using NPC@CNTs and PP batteries. The high discharge capacity and sulfur utilization of the Fe-NPC@CNTs Li-S battery indicates excellent kinetics of the polysulfide conversion reaction. The rate performance of the Li-S battery fabricated with Fe-NPC@CNTs modified separator was 1094, 942, 830, 721 and 631 mAh g^{-1} at 0.5, 1.0, 2.0, 3.0 and 4.0 C, which is faster and larger to other edge-free materials (Figure 11d). Above results indicate that the lithium battery based on the edge-rich Fe-NPC@CNTs modified separator has outstanding energy storage and conversion capabilities as well as good kinetic reversibility.

Table 3. The performance comparison of Ni/H-OMC and recent SA/NCs for the CO_2RR.

Catalysts	FE_{CO} (%)	j_{CO} (mA·cm^{-2})	Potential Window (FE_{CO} > 90%, V vs. RHE)	Stability (h)	Reference
Ni/H-OMC	~100	19.8	−0.5 ~ −1.1	40	[86]
NiNG-S	97	20	−0.7 ~ −0.8	20	[159]
Fe-SAC/NPC	97	2	−0.3 ~ −0.7	24	[160]
Ga-N_3S-PC	92	~20	−0.2 ~ −0.3	24	[161]
Ca-N_3O	97.3	~8.2	−0.65 ~ −1.05	26	[162]
Ni-BNC	98.4	62.9	−0.65 ~ −1.05	27	[163]
Mn–NO/CN	96	2.85	−0.4 ~ −0.5	70	[164]
ACP/S–N–Ni	91	3.4	−0.75 ~ −0.85	14	[165]
Ni-Zn-N-C	99	17	−0.5 ~ −1.0	28	[166]
Cu-Fe-N_6-C	98	4	−0.6 ~ −0.9	10	[167]
Fe_1–Ni_1–N–C	95	2.5	−0.4 ~ −0.6	10	[168]
Fe/Cu–N–C	99.2	12.5	−0.4 ~ −1.1	60	[42]
Co-N-Ni/NPCNSs	96.4	4	−0.48 ~ −0.68	20	[169]
Ni/Fe-N-C	98	8	−0.5 ~ −0.9	30	[170]

Potassium-ion batteries (PIBs) have become a compelling alternative to Li-ion batteries, owing to their abundant potassium resources (2.09 wt.%) and favorable redox potential (K/K^+ = −2.93 V vs. Li/Li^+ = −3.04 V) [171, 172]. Hard carbon was often used as the anode material for PIBs due to its economic applicability and excellent K^+ storage capacity [173, 174]. However, the latest findings exhibited that hard carbon anodes/substrates attained the blockage with their capacity is typically hard to pass 600 mAh g^{-1} [175]. Consequently, various strategies including morphological engineering, heteroatom doping, and graphitization have been employed to improve K^+ storage capacity. Chen et al. initially confirmed that edge structure is an outstanding approach to enhance the K^+ storage in hard carbon by anchoring edge Ni-N_4 sites in B, N co-doped hard carbon nanotubes (Ni@BNHC/CNTs) [176]. The Ni-N_4-B site at the carbon edge can provide active sites for interlayer adsorption of K^+, and the Ni atom can promote the reversible storage of K^+ on the N and B atoms. The charge-discharge curve shows that the initial potassification/depotassification capacity of Ni@BNHC/CNTs (4007/694 mAh g^{-1}) is higher than Ni@BNHC and BNHC (Figure 11e). Ni@BNHC and Ni@BNHC/CNTs exhibit extremely high discharge capacity below 1.0 V, and the dQ/dV charge curve trends of Ni@BNHC and Ni@BNHC/CNTs below 1.5 V are substantially unlike from those of BNHC (Figure 11f). This can be elucidated as the edge Ni-N_4-B sites having additional storage capacity and reversibility for K^+. Ni@BNHC/CNTs exhibit superior K^+ storage performance over Ni@BNHC and BNHC at every specific current, thanks to their enhanced

electron mobility and additional retention of K^+ active sites. Additionally, the reversible capacities of Ni@BNHC/CNTs at 0.1, 0.2, 0.5, 1, 2, 5 and 10 A g^{-1} were 488, 417, 329, 268, 215, 154 and 115 mAh g^{-1}, respectively, which are significantly higher than those of the reported hard carbon materials (Figure 11g) [177-182]. The above data indicate that the hard carbon anode with edge structure assistance has significantly enhanced the storage capacity for K^+, and has broken through the 600 mAh g^{-1} limit.

PIBs have addressed the problems of LIBs, such as the scarcity of lithium resources, high costs, and restricted supply chains, however, in terms of their diffusion kinetics, rate performance, energy density, etc., they still cannot reach the level of LIBs. In the future, the energy band structure and electron transport ability of eSA/NCs should be continuously optimized to promote the commercialization of PIB.

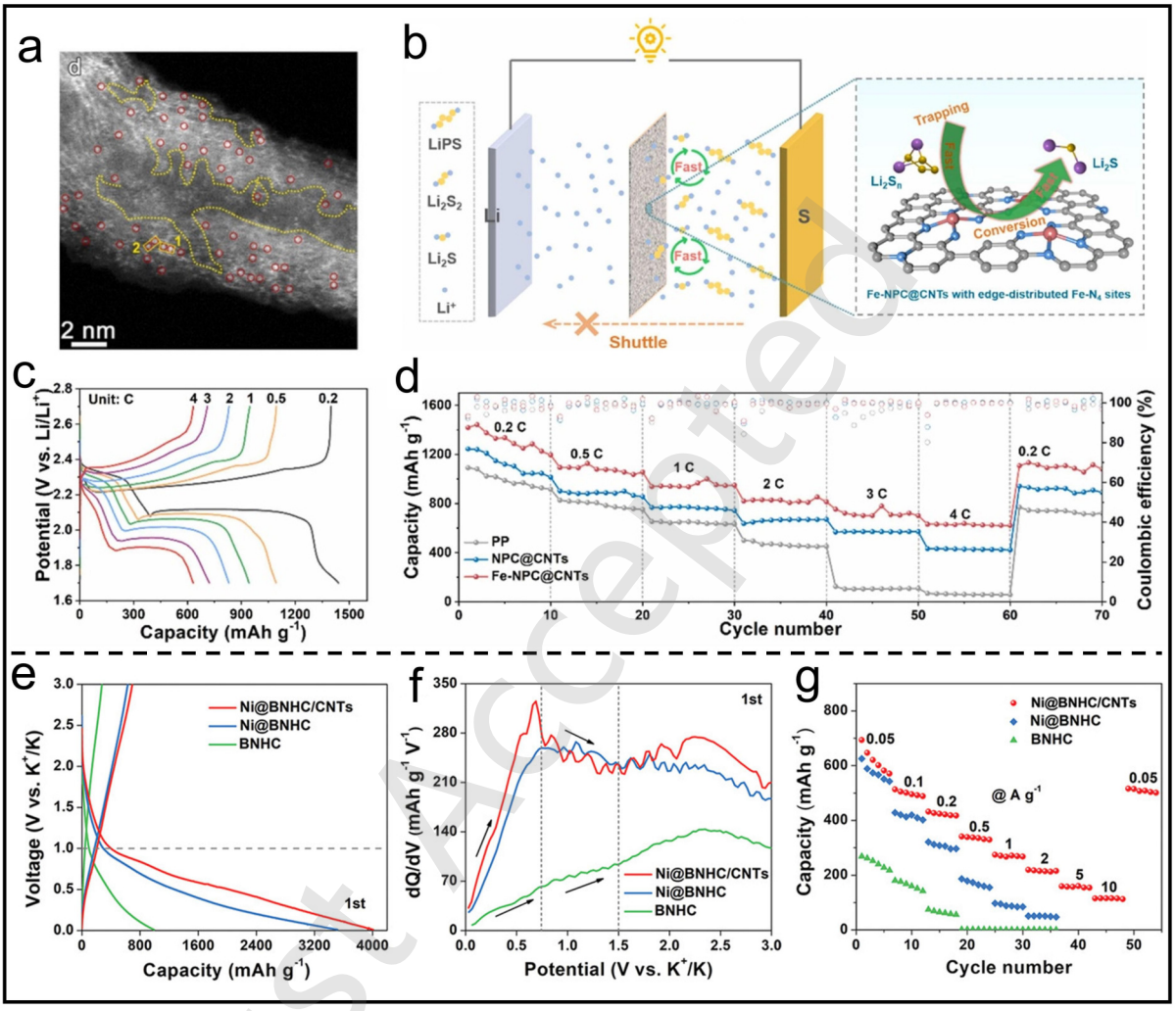

Figure 11. (a) HAADF-STEM image of edge-rich Fe-NPC@CNTs. (b) Graphical representation of the kinetic enhancement mechanism of edge-distributed Fe-N_4 moieties in Li-S battery. (c) Constant current charge/discharge cycles, and (d) stability evaluation at different current densities of Fe-NPC@CNTs. Reproduced with permission from [158]. Copyright 2023, Elsevier. (e) Initial charge/discharge cycles at 0.05 A g^{-1}, (f) related dQ/dV ration curves, and (g) rate assessments of BNHC, Ni@BNHC, and Ni@BNHC/CNTs. Reproduced with permission from [176]. Copyright 2023, Wiley-VCH.

4. Conclusions and perspectives

Designing substrates with rich edge structures can effectively enhance the activity of SA/NCs. This paper reviews the design and synthesis strategies of various eSA/NCs, as well as their applications in different electrochemical reactions. Furthermore, we also summarized and analyzed the characterization methods of edge single atoms sites and the regulation mechanisms of their special geometric and electronic structure characteristics on the charge density and d-band center of the metal center. Despite significant advancements in the study of eSA/NCs for electrocatalysis, challenges remain in achieving controllable preparation of high-density edge sites and their large-scale applications (Figure 12).

Precise regulation of the topological structure of the substrate edge is a key scientific issue in constructing edge-rich eSA/NCs. Among them, the edge proportion and spatial distribution of the carbon substrate directly affect the anchoring efficiency and catalytic activity of the metal site. To advance the research and development of high-density eSA/NCs, it is critical to establish a structure-activity relationship-guided synthetic methodology. This method requires the collaborative work of in-situ characterization and theoretical calculation to guide the preparation of high-density edge single-atom catalysts and the speculation of their catalytic performance.

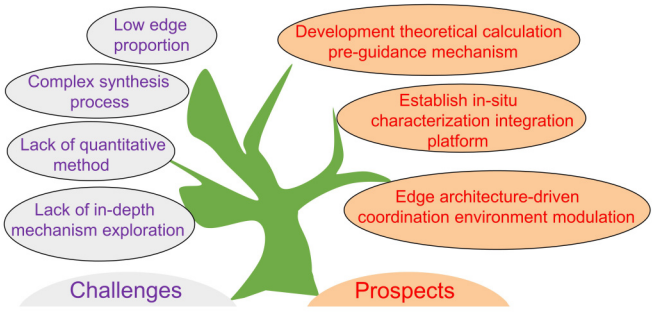

Figure 12. Current challenges and prospects of eSA/NCs.

For the structure-activity analysis of eSA/NCs, it is urgent to establish an in-situ characterization and detection technologies system covering multiple scales from atoms to mesoscopes. At the level of catalytic interface science, the essence of the electrocatalytic process is the interface reaction behavior, and its activity is directly regulated by the precise topological structure of the carbon substrate surface, especially the carbon-based edge single-atom system prepared by high-temperature pyrolysis, its surface often presents complex multi-level structural characteristics. The sub-nanometer structure differences (defect level, curvature strain, and long-distance coordination) may lead to significant deviations between the experimental observations and theoretical predictions. Thereby highlighting the necessity of establishing precise in-situ characterization and detection techniques, including in-situ high-resolution TEM, XAFS, FTIR, and XPS, which can quantitative characterization of multi-dimensional parameters ranging from the defect content and edge proportion on the substrate surface to the binding strength of reaction intermediates and the transformation path.

To elucidate the microscopic mechanism by which edge structures govern single-atom site performance, a multi-scale, interdisciplinary framework integrating theoretical and experimental approaches is essential. DFT-based first-principles calculations serve as a pivotal tool to probe the structural and reactive properties of single-atom sites at carbon edges. Theoretical analysis can clarify how edge structure composition and proportion influence intrinsic properties (e.g., d-band center, charge distribution, spin polarization) and quantitatively assess key parameters like electron transfer pathways and intermediate adsorption energy barriers. This deep integration of theory and experimentation provides a robust foundation for the rational design of eSA/NCs materials and guides the directional optimization of high-density edge-type metal sites. By establishing a deep integration of experiments and theoretical calculations, a solid scientific basis for the rational design of the eSA/NCs and strongly is provided, and guides the directional construction and performance optimization of the high-density edge-type metal sites.

eSA/NCs, as a branch of SACs, are expected to become a key area in future energy conversion research. Despite existing challenges, we remain confident that through innovative approaches, researchers will develop more efficient and refined strategies for fabricating carbon substrates with abundant edge structures. This advancement will enable the preparation of highly stable eSA/NCs exhibiting superior catalytic activity and broader applicability, ultimately contributing to addressing the pressing global challenges of energy scarcity and environmental degradation. We anticipate that this review will stimulate further innovation and advancement in eSA/NCs research, while providing valuable insights for the systematic design of future effective SACs.

Data availability

Not applicable.

Acknowledgements

This work was supported by the National Key R&D Program of China (Nos. 2025YFE0152700), the China Postdoctoral Science Foundation (Nos. 2025M770959), the Basic and Applied Basic Research Foundation of Guangdong province (Nos. 2024A1515110016 and 2023A1515140020), and the National Natural Science Foundation of China (Nos. 52300127).

Declaration of competing interest

The authors declare that they have no competing interests.

Author contribution statement

Chenghong Hu: Conceived the theme and framework, Writing-original draft. **Yuwei Wang, Hafiz Muhammad Adeel Sharif:** Writing- review & editing. **Yang Cai, Linxiao Hou, Xuelei Yan:** Literature search. **Changping Li:** Funding acquisition, Supervision, Project administration.

Use of AI statement

None.

References

[1] Rode, A.; Carleton, T.; Delgado, M.; Greenstone, M.; Houser, T.; Hsiang, S.; Hultgren, A.; Jina, A.; Kopp, R.; McCusker, K.; Nath, I.; Rising, J.; Yuan, J. Estimating a social cost of carbon for global energy consumption. *Nature* **2021**, *598*, 308–314.

[2] Zichittella, G.; Perez-Ramirez, J. Status and prospects of the decentralised valorisation of natural gas into energy and energy carriers. *Chem. Soc. Rev.* **2021**, *50*, 2984–3012.

[3] Mohan, B.; Singh, K.; Gupta, R.; Pombeiro, A.; Ren, P. Advanced materials for energy harvesting: Exploring the potential of MOFs and MXene membranes in osmotic energy applications. *Prog. Mater. Sci.* **2025**, *152*, 101457.

[4] Hu, T.; Zhou, W.; Tang, W. Recent advances and challenges of double-atom catalysts in diverse environmental applications: A state-of-the-art review. *Coord. Chem. Rev.* **2025**, *532*, 216545.

[5] Zhang, Y.; Lin, Y.; Duan, T.; Song, L. Interfacial engineering of heterogeneous catalysts for electrocatalysis. *Mater. Today* **2021**, *48*, 115–134.

[6] Liu, J.; Li, Z.; Lv, C.; Tan, X.-Y.; Lee, C.; Loh, X.; Chua, M.; Li, Z.; Pan, H.; Chen, J.; Zhu, Q.; Xu, J.; Yan, Q. Electrocatalytic upgrading of nitrogenous wastes into value-added chemicals: A review. *Mater. Today* **2024**, *73*, 208–259.

[7] Wu, Y.; Xiao, B.; Liu, K.; Wang, S.; Hou, Y.; Lu, X.; Zhang, J. Electrochemical Synthesis of High-Efficiency Water Electrolysis Catalysts. *Electrochem. Energy Rev.* **2025**, *8*, 2.

[8] Ding, Y.; Cai, P.; Wen, Z. Electrochemical neutralization energy: from concept to devices. *Chem. Soc. Rev.* **2021**, *50*, 1495–1511.

[9] Akhade, S.; Singh, N.; Gutierrez, O.; Lopez-Ruiz, J.; Wang, H.; Holladay, J.; Liu, Y.; Karkamkar, A.; Weber, R.; Padmaperuma, A.; Lee, M.; Whyatt, G.; Elliott, M.; Holladay, J.; Male, J.; Lercher, J.; Rousseau, R.; Glezakou, V. Electrocatalytic Hydrogenation of Biomass-Derived Organics: A Review. *Chem. Rev.* **2020**, *120*, 11370–11419.

[10] Jesudass, S.; Surendran, S.; Janani, G.; Kim, T.; Sim, U.

Redistributing the Electronic States of 2D‐Covalent Organic Frameworks for Electrochemical Energy Applications. *Adv. Energy Mater.* **2023**, *13*, 2301918.
[11] Meng, Z.; Qiu, Z.; Shi, Y.; Wang, S.; Zhang, G.; Pi, Y.; Pang, H. Micro/nano metal–organic frameworks meet energy chemistry: A review of materials synthesis and applications. *eScience* **2023**, *3*, 100092.
[12] Zhang, X.; Li, S.; Zhao, G.; Zhao, H.; Zhou, M. Single-atom catalysts toward electrochemical water treatment. *Appl. Catal. B: Environ. Energy* **2025**, *363*, 124783.
[13] Cai, J.; Javed, R.; Ye, D.; Zhao, H.; Zhang, J. Recent progress in noble metal nanocluster and single atom electrocatalysts for the hydrogen evolution reaction. *J. Mater. Chem. A* **2020**, *8*, 22467–22487.
[14] Lai, J.; Chao, Y.; Zhou, P.; Yang, Y.; Zhang, Y.; Yang, W.; Wu, D.; Feng, J.; Guo, S. One-Pot Seedless Aqueous Design of Metal Nanostructures for Energy Electrocatalytic Applications. *Electrochem. Energy Rev.* **2018**, *1*, 531−547.
[15] Li, B.; Kang, L.; Lun, Y.; Yu, J.; Song, S.; Wang, Y. Structure–performance relationship of Au nanoclusters in electrocatalysis: Metal core and ligand structure. *Carbon Energy* **2024**, *6*, e547.
[16] Li, H.; Li, G. Novel palladium-based nanomaterials for multifunctional ORR/OER/HER electrocatalysis. *J. Mater. Chem. A* **2023**, *11*, 9383–9400.
[17] Li, Y.; Cheng, C.; Han, S.; Huang, Y.; Du, X.; Zhang, B.; Yu, Y. Electrocatalytic Reduction of Low-Concentration Nitric Oxide into Ammonia over Ru Nanosheets. *ACS Energy Lett.* **2022**, *7*, 1187–1194.
[18] Ni, J.-C.; Luan, Y.-X.; Wang, X.-F.; Tan, Z.; Song, X.-Z. Mapping current high-entropy materials for water electrolysis: from noble metal to transition metal. *J. Mater. Chem. A* **2024**, *12*, 14268–14301.
[19] Zhang, B. W.; Yang, H. L.; Wang, Y. X.; Dou, S. X.; Liu, H. K. A Comprehensive Review on Controlling Surface Composition of Pt‐Based Bimetallic Electrocatalysts. *Adv. Energy Mater.* **2018**, *8*, 1703597.
[20] Liu, Y.; Wu, Z.; Gu, C.; Chen, J.; Zhu, Y.; Wang, L. Curved Structure Regulated Single Metal Sites for Advanced Electrocatalytic Reactions. *Small* **2024**, *20*, 2404758.
[21] Wang, H.; Li, X.; Deng, Y.; Jiang, J.; Ma, H.; Zou, J. Advances in MXene-based single-atom catalysts for electrocatalytic applications. *Coord. Chem. Rev.* **2025**, *529*, 216462.
[22] Zhou, B.; Liu, K.; Yu, K.; Zhou, Q.; Gao, Y.; Gao, X.; Chen, Z.; Chen, W.; Chen, P. Ultrafast Synthesis of Single-Atom Catalysts for Electrocatalytic Applications. *Small* **2025**, 2501917.
[23] Liu, J.; Yang, J.; Dou, Y.; Liu, X.; Chen, S.; Wang, D. Deactivation Mechanism and Mitigation Strategies of Single-Atom Site Electrocatalysts. *Adv. Mater.* **2025**, *37*, 2420383.
[24] Liang, X.; Fu, N.; Yao, S.; Li, Z.; Li, Y. The Progress and Outlook of Metal Single-Atom-Site Catalysis. *J. Am. Chem. Soc.* **2022**, *144*, 18155–18174.
[25] Liang, X.; Yao, S.; Li, Z.; Li, Y. Challenge and Chance of Single Atom Catalysis: The Development and Application of the Single Atom Site Catalysts Toolbox. *Acc. Chem. Res.* **2025**, *58*, 1607–1619.
[26] Kment, S.; Bakandritsos, A.; Tantis, I.; Kmentova, H.; Zuo, Y.; Henrotte, O.; Naldoni, A.; Otyepka, M.; Varma, R. S.; Zboril, R. Single Atom Catalysts Based on Earth-Abundant Metals for Energy-Related Applications. *Chem. Rev.* **2024**, *124*, 11767–11847.
[27] Li, S.; Lu, X.; Liu, S.; Zhou, J.; Liu, Y.; Zhang, H.; Shen, R.; Sun, K.; Jiang, J.; Wang, Y.; Li, B. Structure design and electrochemical properties of carbon-based single atom catalysts in energy catalysis: A review. *J. Energy Chem.* **2024**, *98*, 196–236.
[28] Cai, Y.; Xiong, J.; Wang, Y.; Sharif, H. M. A.; Cai, J.; Pan, T.; Tan, X.; Li, Z.; Li, C. Single-atom Pd confined in Ti_3C_2 nanosheet for boosted room-temperature trace NO_2 monitoring. *Nano Res.* **2025**, *18*, 94907285.
[29] Cui, J.; Yu, X.; Li, X.; Yu, J.; Peng, L.; Wei, Z. Advances in spin regulation of M-N-C single-atom catalysts and their applications in electrocatalysis. *Chin. J. Catal.* **2025**, *69*, 17–34.
[30] Kamaruddin, H.; Zhang, J.; Liang, Y.; Wei, Y.; Huang, Y. A review of noble metal-free high entropy alloys for water splitting applications. *J. Mater. Chem. A* **2024**, *12*, 9933–9961.
[31] Li, Y.; Wang, H.; Yang, X.; O'Carroll, T.; Wu, G. Designing and Engineering Atomically Dispersed Metal Catalysts for CO_2 to CO Conversion: From Single to Dual Metal Sites. *Angew. Chem. Int. Ed.* **2024**, *63*, e202317884.
[32] Xin, Y.; Hua, Q.; Li, C.; Zhu, H.; Gao, L.; Ren, X.; Yang, P.; Liu, A. Enhancing electrochemical performance and corrosion resistance of nickel-based catalysts in seawater electrolysis: focusing on OER and HER. *J. Mater. Chem. A* **2024**, *12*, 23147–23178.
[33] Cao, P.; Mu, X.; Chen, F.; Wang, S.; Liao, Y.; Liu, H.; Du, Y.; Li, Y.; Peng, Y.; Gao, M.; Liu, S.; Wang, D.; Dai, Z. Breaking symmetry for better catalysis: insights into single-atom catalyst design. *Chem. Soc. Rev.* **2025**, *54*, 3848–3905.
[34] Mu, X.; Liu, S.; Zhang, M.; Zhuang, Z.; Chen, D.; Liao, Y.; Zhao, H.; Mu, S.; Wang, D.; Dai, Z. Symmetry-Broken Ru Nanoparticles with Parasitic Ru-Co Dual-Single Atoms Overcome the Volmer Step of Alkaline Hydrogen Oxidation. *Angew. Chem. Int. Ed.* **2024**, *63*, e202319618.
[35] Sun, T.; Jian, C.; Wang, G.; Zhao, H.; Zhang, G.; Li, Z.; Li, C. Construction of Ni single-atom coordinated with doped N and S elements for mild hydrogenation of methyl acrylate to methyl propionate. *Nano Res.* **2025**, *18*, 94907053.
[36] Sun, Z.; Li, C.; Wei, Z.; Zhang, F.; Deng, Z.; Zhou, K.; Wang, Y.; Guo, J.; Yang, J.; Xiang, Z.; Ma, P.; Zhai, H.; Li, S.; Chen, W. Sulfur-Bridged Asymmetric CuNi Bimetallic Atom Sites for CO_2 Reduction with High Efficiency. *Adv. Mater.* **2024**, *36*, 2404665.
[37] Wu, H.; Tian, B.; Xu, W.; Abdalla, K. K.; Kuang, Y.; Li, J.; Sun, X. Pressure-Dependent CO_2 Electroreduction to Methane over Asymmetric Cu-N_2 Single-Atom Sites. *J. Am. Chem. Soc.* **2024**, *146*, 22266–22275
[38] Ao, X.; Ding, Y.; Nam, G.; Soule, L.; Jing, P.; Zhao, B.; Hwang, J. Y.; Jang, J. H.; Wang, C.; Liu, M. A Single-Atom Fe-N-C Catalyst with Ultrahigh Utilization of Active Sites for Efficient Oxygen Reduction. *Small* **2022**, *18*, 2203326.
[39] Chen, W.; Ma, B.; Zou, R. Rational Design and Controlled Synthesis of MOF-Derived Single-Atom Catalysts. *Acc. Mater. Res.* **2025**, *6*, 210–220.
[40] Lu, X.; Li, Y.; Dong, D.; Wan, Y.; Li, R.; Xiao, L.; Wang, D.; Liu, L.; Wang, G.; Zhang, J.; An, M.; Yang, P. Coexisting Fe single atoms and nanoparticles on hierarchically porous carbon for high-efficiency oxygen reduction reaction and Zn-air batteries. *J. Colloid. Interface Sci.* **2024**, *653*, 654–663.
[41] Ma, G.; Chen, Y.; Li, H.; Sun, Y.; Fan, H.; Jiang, S.; Cui, X.; Ma, T. Hierarchically porous N-doped carbon confined single-atom Fe catalyst for efficient electrochemical CO_2 reduction. *Nano Res.* **2025**, *18*, 94907297.
[42] Feng, M.; Wu, X.; Cheng, H.; Fan, Z.; Li, X.; Cui, F.; Fan, S.; Dai, Y.; Lei, G.; He, G. Well-defined Fe–Cu diatomic sites for efficient catalysis of CO_2 electroreduction. *J. Mater. Chem. A* **2021**, *9*, 23817–23827.
[43] Han, Y.; Wang, Y.; Xu, R.; Chen, W.; Zheng, L.; Han, A.; Zhu, Y.; Zhang, J.; Zhang, H.; Luo, J.; Chen, C.; Peng, Q.; Wang, D.; Li, Y. Electronic structure engineering to boost oxygen reduction activity by controlling the coordination of the central metal. *Energy Environ. Sci.* **2018**, *11*, 2348–2352.
[44] Hu, C.; Wang, Y.; Chen, J.; Wang, H. F.; Shen, K.; Tang, K.; Chen, L.; Li, Y. Main-Group Metal Single-Atomic Regulators in Dual-Metal Catalysts for Enhanced Electrochemical CO_2 Reduction. *Small* **2022**, *18*, 2201391.
[45] Hu, C.; Zhang, Y.; Zhang, Y.; Huang, Q.; Shen, K.; Chen, L.; Li, Y. Single-atomic Fe sites modulated by Sn regulator for enhanced electrochemical CO_2 reduction. *Chin. J. Catal.* **2025**, *72*, 222–229.
[46] Hu, L.; Dai, C.; Chen, L.; Zhu, Y.; Hao, Y.; Zhang, Q.; Gu, L.; Feng, X.; Yuan, S.; Wang, L.; Wang, B. Metal-Triazolate-Framework-Derived FeN_4Cl_1 Single-Atom Catalysts with Hierarchical Porosity for the Oxygen Reduction Reaction. *Angew. Chem. Int. Ed.* **2021**, *60*, 27324–27329.
[47] Sun, X.; Tuo, Y.; Ye, C.; Chen, C.; Lu, Q.; Li, G.; Jiang, P.; Chen, S.; Zhu, P.; Ma, M.; Zhang, J.; Bitter, J.; Wang, D.; Li, Y. Phosphorus Induced Electron Localization of Single Iron Sites for Boosted CO_2 Electroreduction Reaction. *Angew. Chem. Int. Ed.* **2021**, *60*, 23614–23618.
[48] Wang, Y.; Ma, F.; Zhang, G.; Zhang, J.; Zhao, H.; Dong, Y.; Wang, D. Precise synthesis of dual atom sites for electrocatalysis. *Nano Res.* **2024**, *17*, 9397–9427.
[49] Wu, Y.; Chen, C.; Yan, X.; Sun, X.; Zhu, Q.; Li, P.; Li, Y.; Liu, S.; Ma, J.; Huang, Y.; Han, B. Boosting CO_2 Electroreduction over a Cadmium Single-Atom Catalyst by Tuning of the Axial Coordination Structure. *Angew. Chem. Int. Ed.* **2021**, *60*, 20803–20810.
[50] Zhu, Z.; Yin, H.; Wang, Y.; Chuang, C. H.; Xing, L.; Dong, M.; Lu, Y. R.; Casillas-Garcia, G.; Zheng, Y.; Chen, S.; Dou, Y.; Liu, P.; Cheng, Q.; Zhao, H. Coexisting Single-Atomic Fe and Ni Sites on Hierarchically Ordered Porous Carbon as a Highly Efficient ORR Electrocatalyst. *Adv. Mater.* **2020**, *32*, 2004670.
[51] Ying, Y.; Fan, K.; Lin, Z.; Huang, H. Facing the "Cutting Edge:" Edge Site Engineering on 2D Materials for Electrocatalysis and Photocatalysis. *Adv. Mater.* **2025**, *37*, 2418757.
[52] Zhao, Y.; Jiang, W. J.; Zhang, J.; Lovell, E. C.; Amal, R.; Han, Z.; Lu, X. Anchoring Sites Engineering in Single-Atom Catalysts for Highly Efficient Electrochemical Energy Conversion Reactions. *Adv. Mater.* **2021**, *33*, 2102801.
[53] Liao, L.; Xia, G.; Wang, Y.; Ye, G.; Wang, H. In-situ N-defect and single-metal atom synergetic engineering of high-efficiency Ag–N–C electrocatalysts for CO_2 reduction. *Appl. Catal. B: Environ.* **2022**, *318*, 121826.
[54] Liu, J.; Gong, Z.; Allen, C.; Ge, W.; Gong, H.; Liao, J.; Liu, J.; Huang, K.; Yan, M.; Liu, R.; He, G.; Dong, J.; Ye, G.; Fei, H. Edge-hosted

Fe-N_3 sites on a multiscale porous carbon framework combining high intrinsic activity with efficient mass transport for oxygen reduction. *Chem Catal.* **2021**, *1*, 1291–1307.
[55] Yin, H.; Yuan, P.; Lu, B.-A.; Xia, H.; Guo, K.; Yang, G.; Qu, G.; Xue, D.; Hu, Y.; Cheng, J.; Mu, S.; Zhang, J.-N. Phosphorus-Driven Electron Delocalization on Edge-Type FeN_4 Active Sites for Oxygen Reduction in Acid Medium. *ACS Catal.* **2021**, *11*, 12754–12762.
[56] Liu, Y.; Liu, X.; Jadhav, A.; Yang, T.; Hwang, Y.; Wang, H.; Wang, L.; Luo, Y.; Kumar, A.; Lee, J.; Bui, H. T. D.; Gyu Kim, M.; Lee, H. Unraveling the Function of Metal-Amorphous Support Interactions in Single-Atom Electrocatalytic Hydrogen Evolution. *Angew. Chem. Int. Ed.* **2022**, *61*, e202114160.
[57] Gloag, L.; Somerville, S.; Gooding, J.; Tilley, R. Co-catalytic metal–support interactions in single-atom electrocatalysts. *Nat. Rev. Mater.* **2024**, *9*, 173–189.
[58] Humayun, M.; Israr, M.; Li, Z.; Luo, W.; Wang, C. Metal oxides confine single atoms toward efficient thermal catalysis. *Coord. Chem. Rev.* **2023**, *488*, 215189.
[59] Fiorio, J.; Garcia, M.; Gothe, M.; Galvan, D.; Troise, P.; Conte-Junior, C.; Vidinha, P.; Camargo, P.; Rossi, L. Recent advances in the use of nitrogen-doped carbon materials for the design of noble metal catalysts. *Coord. Chem. Rev.* **2023**, *481*, 215053.
[60] Rocha, G.; da Silva, M.; Rogolino, A.; Diab, G.; Noleto, L.; Antonietti, M.; Teixeira, I. Carbon nitride based materials: more than just a support for single-atom catalysis. *Chem. Soc. Rev.* **2023**, *52*, 4878–4932.
[61] Wang, S.; Dong, Y.; Fu, Y.; Li, B.; Zhang, J. Microenvironment engineering in carbon nitride supported metal single atoms for solar driven aqueous pollutant removal. *Chem. Eng. J.* **2025**, *504*, 158759.
[62] Hu, J.; Shang, W.; Xin, C.; Guo, J.; Cheng, X.; Zhang, S.; Song, S.; Liu, W.; Ju, F.; Hou, J.; Shi, Y. Uncovering Dynamic Edge-Sites in Atomic Co-N-C Electrocatalyst for Selective Hydrogen Peroxide Production. *Angew. Chem. Int. Ed.* **2023**, *62*, e202304754.
[63] Noh, W.; Mun, J.; Lee, Y.; Kim, E.; Kim, Y.; Kim, K.; Jeong, H.; Lee, J.; Song, H.; Lee, G.; Lee, J. Molecularly Engineered Carbon Platform To Anchor Edge-Hosted Single-Atomic M–N/C (M = Fe, Co, Ni, Cu) Electrocatalysts of Outstanding Durability. *ACS Catal.* **2022**, *12*, 7994–8006.
[64] Zhou, Y.; Xie, M.; Song, Y.; Yan, D.; Wang, Z.; Zhang, S.; Deng, C. Edge-enriched Ni-N_4 atomic sites embedded enoki-mushroom-like carbon nanotubes assembling hollow fibers for CO_2 conversion and flexible Zn-air battery. *Energy Storage Mater.* **2022**, *47*, 235–248.
[65] Xiao, M.; Xing, Z.; Jin, Z.; Liu, C.; Ge, J.; Zhu, J.; Wang, Y.; Zhao, X.; Chen, Z. Preferentially Engineering FeN_4 Edge Sites onto Graphitic Nanosheets for Highly Active and Durable Oxygen Electrocatalysis in Rechargeable Zn-Air Batteries. *Adv. Mater.* **2020**, *32*, 2004900.
[66] Wang, X.; Jia, Y.; Mao, X.; Liu, D.; He, W.; Li, J.; Liu, J.; Yan, X.; Chen, J.; Song, L.; Du, A.; Yao, X. Edge-Rich Fe-N_4 Active Sites in Defective Carbon for Oxygen Reduction Catalysis. *Adv. Mater.* **2020**, *32*, 2000966.
[67] Song, Z.; Zhang, L.; Doyle‐Davis, K.; Fu, X.; Luo, J. L.; Sun, X. Recent Advances in MOF‐Derived Single Atom Catalysts for Electrochemical Applications. *Adv. Energy Mater.* **2020**, *10*, 2001561.
[68] Wang, K.; Li, Y.; Xie, L. H.; Li, X.; Li, J. R. Construction and application of base-stable MOFs: a critical review. *Chem. Soc. Rev.* **2022**, *51*, 6417–6441.
[69] Lin, D.; Lin, X.; Li, H.; Huang, H.; Yang, H.; Yang, J.; Hu, B.; Chen, F.; Guo, X.; Wang, X.; Yao, W. Ultrathin porous nitrogen-doped carbon nanosheets with rich defects for efficient Cr(VI) reduction. *Appl. Catal. B: Environ. Energy* **2025**, *370*, 125174.
[70] Xin, Y.; Cao, Y.; Yang, J.; Guo, X.; Shen, K.; Yao, W. Mesopore and macropore engineering in metal–organic frameworks for energy environment-related applications. *J. Mater. Chem. A* **2024**, *12*, 4931–4970.
[71] Karapinar, D.; Huan, N.; Ranjbar Sahraie, N.; Li, J.; Wakerley, D.; Touati, N.; Zanna, S.; Taverna, D.; Galvao Tizei, L.; Zitolo, A.; Jaouen, F.; Mougel, V.; Fontecave, M. Electroreduction of CO_2 on Single-Site Copper-Nitrogen-Doped Carbon Material: Selective Formation of Ethanol and Reversible Restructuration of the Metal Sites. *Angew. Chem. Int. Ed.* **2019**, *58*, 15098–15103.
[72] Shang, H.; Wang, T.; Pei, J.; Jiang, Z.; Zhou, D.; Wang, Y.; Li, H.; Dong, J.; Zhuang, Z.; Chen, W.; Wang, D.; Zhang, J.; Li, Y. Design of a Single-Atom Indium$^{\delta+}$-N_4 Interface for Efficient Electroreduction of CO_2 to Formate. *Angew. Chem. Int. Ed.* **2020**, *59*, 22465–22469.
[73] Ding, T.; Liu, X.; Tao, Z.; Liu, T.; Chen, T.; Zhang, W.; Shen, X.; Liu, D.; Wang, S.; Pang, B.; Wu, D.; Cao, L.; Wang, L.; Liu, T.; Li, Y.; Sheng, H.; Zhu, M.; Yao, T. Atomically Precise Dinuclear Site Active toward Electrocatalytic CO_2 Reduction. *J. Am. Chem. Soc.* **2021**, *143*, 11317–11324
[74] Cheng, H.; Wu, X.; Feng, M.; Li, X.; Lei, G.; Fan, Z.; Pan, D.; Cui, F.; He, G. Atomically Dispersed Ni/Cu Dual Sites for Boosting the CO_2 Reduction Reaction. *ACS Catal.* **2021**, *11*, 12673–12681.
[75] Zhang, R.; Xue, B.; Tao, Y.; Zhao, H.; Zhang, Z.; Wang, X.; Zhou, X.; Jiang, B.; Yang, Z.; Yan, X.; Fan, K. Edge-Site Engineering of Defective Fe-N_4 Nanozymes with Boosted Catalase-Like Performance for Retinal Vasculopathies. *Adv. Mater.* **2022**, *34*, 2205324.
[76] Yin, Y.; Rioux, R.; Erdonmez, C.; Hughes, S.; Somorjai, G.; Alivisatos, A. Formation of Hollow Nanocrystals Through the Nanoscale Kirkendall Effect. *Science* **2004**, *304*, 711–714.
[77] Jiang, R.; Li, L.; Sheng, T.; Hu, G.; Chen, Y.; Wang, L. Edge-Site Engineering of Atomically Dispersed Fe-N_4 by Selective C-N Bond Cleavage for Enhanced Oxygen Reduction Reaction Activities. *J. Am. Chem. Soc.* **2018**, *140*, 11594–11598.
[78] Zhang, P.; Guan, B. Y.; Yu, L.; Lou, X. W. Facile Synthesis of Multi-shelled ZnS-CdS Cages with Enhanced Photoelectrochemical Performance for Solar Energy Conversion. *Chem* **2018**, *4*, 162–173.
[79] Huang, J.; Chen, J.; Liu, W.; Zhang, J.; Chen, J.; Li, Y. Copper-doped zinc sulfide nanoframes with three-dimensional photocatalytic surfaces for enhanced solar driven H_2 production. *Chin. J. Catal.* **2022**, *43*, 782–792.
[80] Kong, F.; Huang, Y.; Chen, M.; Meng, G.; Tian, H.; Chen, Y.; Chang, Z.; Chen, C.; Sun, W.; Cui, X.; Shi, J. Creation of densely exposed and cavity-edged single Fe active sites for enhanced oxygen electroreduction. *Appl. Catal. B: Environ.* **2022**, *317*, 121768.
[81] Yu, X.; Liu, H.; Huang, Y.; Li, C.; Kuang, L.; Zhong, J.; Zhu, S.; Gou, Y.; Wang, Y.; Zhang, Y.; Shan, G.; Lv, Z.; Zhang, S.; Zhu, L. A green edge-hosted zinc single-site heterogeneous catalyst for superior Fenton-like activity. *P. Natl. Acad. Sci.* **2023**, *120*, e2221228120.
[82] Daiyan, R.; Tan, X.; Chen, R.; Saputera, W. H.; Tahini, H. A.; Lovell, E.; Ng, Y. H.; Smith, S. C.; Dai, L.; Lu, X.; Amal, R. Electroreduction of CO_2 to CO on a Mesoporous Carbon Catalyst with Progressively Removed Nitrogen Moieties. *ACS Energy Lett.* **2018**, *3*, 2292–2298.
[83] Ni, W.; Liu, Z.; Zhang, Y.; Ma, C.; Deng, H.; Zhang, S.; Wang, S. Electroreduction of Carbon Dioxide Driven by the Intrinsic Defects in the Carbon Plane of a Single Fe-N_4 Site. *Adv. Mater.* **2021**, *33*, 2003238.
[84] Wang, X.; Han, X.; Du, R.; Liang, Z.; Zuo, Y.; Guardia, P.; Li, J.; Llorca, J.; Arbiol, J.; Zheng, R.; Cabot, A. Unveiling the role of counter-anions in amorphous transition metal-based oxygen evolution electrocatalysts. *Appl. Catal. B: Environ.* **2023**, *320*, 121988.
[85] Wu, Z.; Wang, L.; Chen, S.; Zhu, X.; Deng, Q.; Wang, J.; Zeng, Z.; Deng, S. Facile and low-temperature strategy to prepare hollow ZIF-8/CNT polyhedrons as high-performance lithium-sulfur cathodes. *Chem. Eng. J.* **2021**, *404*, 126579.
[86] Hu, C.; Hong, X.; Liu, M.; Shen, K.; Chen, L.; Li, Y. Hierarchically Ordered Pore Engineering of Carbon Supports with High-Density Edge-Type Single-Atom Sites to Boost Electrochemical CO_2 Reduction. *Adv. Mater.* **2024**, *36*, 2409531.
[87] Yao, W.; Hu, C.; Zhang, Y.; Li, H.; Wang, F.; Shen, K.; Chen, L.; Li, Y. Hierarchically ordered porous carbon with atomically dispersed cobalt for oxidative esterification of furfural. *Ind. Chem. Mater.* **2023**, *1*, 106–116.
[88] Hu, C.; Yao, W.; Yang, X.; Shen, K.; Chen, L.; Li, Y. Atomically Dispersed ZnN_4 Sites Anchored on P-Functionalized Carbon with Hierarchically Ordered Porous Structures for Boosted Electroreduction of CO_2. *Adv. Sci.* **2024**, *11*, 2306095.
[89] Kim, K.; Lee, J.; Park, O.; Kim, J.; Kim, J.; Lee, D.; Paidi, V.; Jung, E.; Lee, H.; Lee, B.; Lee, C.; Ko, W.; Lee, K.; Jung, Y.; Lee, C.; Lee, N.; Back, S.; Choi, S.; Hyeon, T. Geometric Tuning of Single-Atom FeN_4 Sites via Edge-Generation Enhances Multi-Enzymatic Properties. *Adv. Mater.* **2023**, *35*, 2207666.
[90] Cheng, Y.-T.; Peng, J.-Z.; Lai, G.-T.; Yue, X.; Li, F.-Z.; Wang, Q.; Chen, L.-N.; Gu, J. Edge-Site Co–Nx Model Single-Atom Catalysts for CO_2 Electroreduction. *ACS Catal.* **2024**, *14*, 8446–8455.
[91] Xie, C.; Yan, D.; Chen, W.; Zou, Y.; Chen, R.; Zang, S.; Wang, Y.; Yao, X.; Wang, S. Insight into the design of defect electrocatalysts: From electronic structure to adsorption energy. *Mater. Today* **2019**, *31*, 47–68.
[92] Qiu, X.; Wang, R. From construction strategies to applications: Multifunctional defective metal-organic frameworks. *Coord. Chem. Rev.* **2025**, *526*, 216356.
[93] Pan, F.; Li, B.; Sarnello, E.; Fei, Y.; Feng, X.; Gang, Y.; Xiang, X.; Fang, L.; Li, T.; Hu, Y.; Wang, G.; Li, Y. Pore-Edge Tailoring of Single-Atom Iron–Nitrogen Sites on Graphene for Enhanced CO_2 Reduction. *ACS Catal.* **2020**, *10*, 10803–10811.
[94] Tang, B.; Ji, Q.; Zhang, X.; Shi, R.; Ma, J.; Zhuang, Z.; Sun, M.; Wang, H.; Liu, R.; Liu, H.; Wang, C.; Guo, Z.; Lu, L.; Jiang, P.; Wang, D.; Yan, W. Symmetry Breaking of FeN_4 Moiety via Edge Defects for Acidic Oxygen Reduction Reaction. *Angew Chem. Int. Ed.* **2025**, *64*, e202424135.
[95] Ye, G.; Liu, S.; Zhao, K.; He, Z. Singlet Oxygen Induced Site-Specific Etching Boosts Nitrogen-Carbon Sites for High-Efficiency Oxygen

Reduction. *Angew Chem. Int. Ed.* **2023**, *62*, e202303409.
[96] Ren, C.; Cui, Y.; Li, Q.; Ling, C.; Wang, J. Single-Atom Saturation: A Fundamental Principle for Single-Atom-Site Catalyst Design. *J. Am. Chem. Soc.* **2025**, *147*, 13610−13617.
[97] Li, H.; Lin, Y.; Duan, J.; Wen, Q.; Liu, Y.; Zhai, T. Stability of electrocatalytic OER: from principle to application. *Chem. Soc. Rev.* **2024**, *53*, 10709−10740.
[98] Kawashima, K.; Marquez, R.; Smith, L.; Vaidyula, R.; Carrasco-Jaim, O.; Wang, Z.; Son, Y.; Cao, C.; Mullins, C. A Review of Transition Metal Boride, Carbide, Pnictide, and Chalcogenide Water Oxidation Electrocatalysts. *Chem. Rev.* **2023**, *123*, 12795−13208.
[99] Shahzad, A.; Zulfiqar, F.; Arif Nadeem, M. Cobalt containing bimetallic ZIFs and their derivatives as OER electrocatalysts: A critical review. *Coord. Chem. Rev.* **2023**, *477*, 214925.
[100] Zeng, F.; Mebrahtu, C.; Liao, L.; Beine, A.; Palkovits, R. Stability and deactivation of OER electrocatalysts: A review. *J. Energy Chem.* **2022**, *69*, 301–329.
[101] Chen, M.; Kitiphatpiboon, N.; Feng, C.; Abudula, A.; Ma, Y.; Guan, G. Recent progress in transition-metal-oxide-based electrocatalysts for the oxygen evolution reaction in natural seawater splitting: A critical review. *eScience* **2023**, *3*, 100111.
[102] Gan, R.; Wang, Y.; Zhang, X.; Song, Y.; Shi, J.; Ma, C. Edge atomic Fe sites decorated porous graphitic carbon as an efficient bifunctional oxygen catalyst for Zinc-air batteries. *J. Energy Chem.* **2023**, *83*, 602–611.
[103] Cheng, Y.; Zhao, S.; Li, H.; He, S.; Veder, J.-P.; Johannessen, B.; Xiao, J.; Lu, S.; Pan, J.; Chisholm, M. F.; Yang, S.-Z.; Liu, C.; Chen, J. G.; Jiang, S. P. Unsaturated edge-anchored Ni single atoms on porous microwave exfoliated graphene oxide for electrochemical CO_2. *Appl. Catal. B: Environ.* **2019**, *243*, 294–303
[104] Yan, C.; Li, H.; Ye, Y.; Wu, H.; Cai, F.; Si, R.; Xiao, J.; Miao, S.; Xie, S.; Yang, F.; Li, Y.; Wang, G.; Bao, X. Coordinatively unsaturated nickel–nitrogen sites towards selective and high-rate CO_2 electroreduction. *Energy Environ. Sci.* **2018**, *11*, 1204–1210
[105] Chen, J.; Li, H.; Fan, C.; Meng, Q.; Tang, Y.; Qiu, X.; Fu, G.; Ma, T. Dual Single-Atomic Ni-N_4 and Fe-N_4 Sites Constructing Janus Hollow Graphene for Selective Oxygen Electrocatalysis. *Adv. Mater.* **2020**, *32*, 2003134.
[106] Yan, L.; Xu, Y.; Chen, P.; Zhang, S.; Jiang, H.; Yang, L.; Wang, Y.; Zhang, L.; Shen, J.; Zhao, X.; Wang, L. A Freestanding 3D Heterostructure Film Stitched by MOF-Derived Carbon Nanotube Microsphere Superstructure and Reduced Graphene Oxide Sheets: A Superior Multifunctional Electrode for Overall Water Splitting and Zn-Air Batteries. *Adv. Mater.* **2020**, *32*, 2003313.
[107] Ge, H.; Li, G.; Shen, J.; Ma, W.; Meng, X.; Xu, L. Co_4N nanoparticles encapsulated in N-doped carbon box as tri-functional catalyst for Zn-air battery and overall water splitting. *Appl. Catal. B: Environ.* **2020**, *275*, 119104.
[108] Han, X.; Ling, X.; Yu, D.; Xie, D.; Li, L.; Peng, S.; Zhong, C.; Zhao, N.; Deng, Y.; Hu, W. Atomically Dispersed Binary Co-Ni Sites in Nitrogen-Doped Hollow Carbon Nanocubes for Reversible Oxygen Reduction and Evolution. *Adv. Mater.* **2019**, *31*, 1905622.
[109] Peng, W.; Yang, X.; Mao, L.; Jin, J.; Yang, S.; Zhang, J.; Li, G. ZIF-67-derived Co nanoparticles anchored in N doped hollow carbon nanofibers as bifunctional oxygen electrocatalysts. *Chem. Eng. J.* **2021**, *407*, 127157.
[110] Wang, R.; Yang, H.; Lu, N.; Lei, S.; Jia, D.; Wang, Z.; Liu, Z.; Wu, X.; Zheng, H.; Ali, S.; Ma, F.; Peng, S. Precise identification of active sites of a high bifunctional performance 3D Co/N-C catalyst in Zinc-air batteries. *Chem. Eng. J.* **2022**, *433*, 134500.
[111] Xie, W.; Song, Y.; Li, S.; Li, J.; Yang, Y.; Liu, W.; Shao, M.; Wei, M. Single‐Atomic‐Co Electrocatalysts with Self‐Supported Architecture toward Oxygen‐Involved Reaction. *Adv. Funct. Mater.* **2019**, *29*, 1906477.
[112] Wang, X.; Zhang, J.; Ma, D.; Feng, X.; Wang, L.; Wang, B. Metal-Organic Framework-Derived Trimetallic Nanocomposites as Efficient Bifunctional Oxygen Catalysts for Zinc-Air Batteries. *ACS Appl. Mater. Interfaces* **2021**, *13*, 33209−33217.
[113] Ding, J.; Liu, W.; Zhang, S.; Luo, J.; Liu, X. A Mini Review: Recent Advances in Asymmetrically Coordinated Atom Sites for High-Efficiency Hydrogen Evolution Reaction. *Energies* **2023**, *16*, 2664.
[114] Hossain, M.; Zhang, L.; Neagu, R.; Sun, S. Exploring the properties, types, and performance of atomic site catalysts in electrochemical hydrogen evolution reactions. *Chem. Soc. Rev.* **2025**, *54*, 3323–3386.
[115] Lang, C.; Xu, Y.; Yao, X. Perfecting HER catalysts via defects: Recent advances and perspectives. *Chin. J. Catal.* **2024**, *64*, 4–31.
[116] Zhang, H.; Zhou, W.; Lu, X.; Chen, T.; Lou, X. Implanting Isolated Ru Atoms into Edge‐Rich Carbon Matrix for Efficient Electrocatalytic Hydrogen Evolution. *Adv. Energy Mater.* **2020**, *10*, 2000882.
[117] Greeley, J.; Jaramillo, T.; Bonde, J.; Chorkendorff, I.; Norskov, J. Computational high-throughput screening of electrocatalytic materials for hydrogen evolution. *Nat. Mater.* **2006**, *5*, 909–913.
[118] Wang, J.; Wei, Z.; Mao, S.; Li, H.; Wang, Y. Highly uniform Ru nanoparticles over N-doped carbon: pH and temperature-universal hydrogen release from water reduction. *Energy Environ. Sci.* **2018**, *11*, 800–806.
[119] Liu, M.; Pang, Y.; Zhang, B.; De Luna, P.; Voznyy, O.; Xu, J.; Zheng, X.; Dinh, C.; Fan, F.; Cao, C.; de Arquer, F.; Safaei, T.; Mepham, A.; Klinkova, A.; Kumacheva, E.; Filleter, T.; Sinton, D.; Kelley, S.; Sargent, E. Enhanced electrocatalytic CO_2 reduction via field-induced reagent concentration. *Nature* **2016**, *537*, 382–386.
[120] Jiao, Y.; Zheng, Y.; Jaroniec, M.; Qiao, S. Z. Design of electrocatalysts for oxygen- and hydrogen-involving energy conversion reactions. *Chem. Soc. Rev.* **2015**, *44*, 2060–2086.
[121] Liang, Z.; Lei, H.; Zheng, H.; Wang, H.; Zhang, W.; Cao, R. Selective two-electron and four-electron oxygen reduction reactions using Co-based electrocatalysts. *Chem. Soc. Rev.* **2025**, *54*, 5248−5291.
[122] Xu, H.; Ma, Z.; Wan, Z.; An, Z.; Wang, X. Recent advances and prospects of iron-based noble metal-free catalysts for oxygen reduction reaction in acidic environment: A mini review. *Int. J. Hydrogen Energy* **2024**, *59*, 697–714.
[123] Zhang, J.; Zhang, J.; He, F.; Chen, Y.; Zhu, J.; Wang, D.; Mu, S.; Yang, H. Y. Defect and Doping Co-Engineered Non-Metal Nanocarbon ORR Electrocatalyst. *Nano-Micro Lett.* **2021**, *13*, 65.
[124] Song, K.; Yang, B.; Zou, X.; Zhang, W.; Zheng, W. Unified ORR mechanism criteria via charge–spin–coordination of Fe functional units. *Energy Environ. Sci.* **2024**, *17*, 27–48
[125] Zhao, J.; Lian, J.; Zhao, Z.; Wang, X.; Zhang, J. A Review of In-Situ Techniques for Probing Active Sites and Mechanisms of Electrocatalytic Oxygen Reduction Reactions. *Nano-Micro Lett.* **2022**, *15*, 19.
[126] Xu, Y.; Sun, Z.; Fan, S.; Han, X.; Li, L.; Gao, Z.; Wang, C. From structure to function: MOF-based and COF-based catalysts for efficient electrocatalytic H_2O_2 production via $2e^-$ ORR. *J. Mater. Chem. A* **2024**, *12*, 27180–27205.
[127] Zhang, P.; Chen, H. C.; Zhu, H.; Chen, K.; Li, T.; Zhao, Y.; Li, J.; Hu, R.; Huang, S.; Zhu, W.; Liu, Y.; Pan, Y. Inter-site structural heterogeneity induction of single atom Fe catalysts for robust oxygen reduction. *Nat. Commun.* **2024**, *15*, 2062.
[128] Li, Z.; Zhuang, Z.; Lv, F.; Zhu, H.; Zhou, L.; Luo, M.; Zhu, J.; Lang, Z.; Feng, S.; Chen, W.; Mai, L.; Guo, S. The Marriage of the FeN_4 Moiety and MXene Boosts Oxygen Reduction Catalysis: Fe 3d Electron Delocalization Matters. *Adv. Mater.* **2018**, *30*, 1803220.
[129] Xiao, M.; Zhu, J.; Li, S.; Li, G.; Liu, W.; Deng, Y.-P.; Bai, Z.; Ma, L.; Feng, M.; Wu, T.; Su, D.; Lu, J.; Yu, A.; Chen, Z. 3d-Orbital Occupancy Regulated Ir-Co Atomic Pair Toward Superior Bifunctional Oxygen Electrocatalysis. *ACS Catal.* **2021**, *11*, 8837–8846.
[130] Tian, Y.; Li, M.; Wu, Z.; Sun, Q.; Yuan, D.; Johannessen, B.; Xu, L.; Wang, Y.; Dou, Y.; Zhao, H.; Zhang, S. Edge-hosted Atomic Co-N_4 Sites on Hierarchical Porous Carbon for Highly Selective Two-electron Oxygen Reduction Reaction. *Angew. Chem. Int. Ed.* **2022**, *61*, e202213296.
[131] Zhang, F.; Zhu, Y.; Tang, C.; Chen, Y.; Qian, B.; Hu, Z.; Chang, Y. C.; Pao, C. W.; Lin, Q.; Kazemi, S.; Wang, Y.; Zhang, L.; Zhang, X.; Wang, H. High‐Efficiency Electrosynthesis of Hydrogen Peroxide from Oxygen Reduction Enabled by a Tungsten Single Atom Catalyst with Unique Terdentate N_1O_2 Coordination. *Adv. Funct. Mater.* **2021**, *32*, 2110224.
[132] Tang, C.; Chen, L.; Li, H.; Li, L.; Jiao, Y.; Zheng, Y.; Xu, H.; Davey, K.; Qiao, S. Z. Tailoring Acidic Oxygen Reduction Selectivity on Single-Atom Catalysts via Modification of First and Second Coordination Spheres. *J. Am. Chem. Soc.* **2021**, *143*, 7819–7827.
[133] Jung, E.; Shin, H.; Lee, B.; Efremov, V.; Lee, S.; Lee, H.; Kim, J.; Hooch Antink, W.; Park, S.; Lee, K.; Cho, S.; Yoo, J.; Sung, Y.; Hyeon, T. Atomic-level tuning of Co-N-C catalyst for high-performance electrochemical H_2O_2 production. *Nat. Mater.* **2020**, *19*, 436–442
[134] Zhang, W.; Fu, Q.; Luo, Q.; Sheng, L.; Yang, J. Understanding Single-Atom Catalysis in View of Theory. *JACS Au* **2021**, *1*, 2130–2145.
[135] Sun, X.; Wei, P.; Gu, S.; Zhang, J.; Jiang, Z.; Wan, J.; Chen, Z.; Huang, L.; Xu, Y.; Fang, C.; Li, Q.; Han, J.; Huang, Y. Atomic-Level Fe-N-C Coupled with Fe(3) C-Fe Nanocomposites in Carbon Matrixes as High-Efficiency Bifunctional Oxygen Catalysts. *Small* **2020**, *16*, 1906057.
[136] Bai, L.; Duan, Z.; Wen, X.; Guan, J. Bifunctional atomic iron-based catalyst for oxygen electrode reactions. *J. Catal.* **2019**, *378*, 353−362
[137] Lai, Q.; Su, Q.; Gao, Q.; Liang, Y.; Wang, Y.; Yang, Z.; Zhang, X.; He, J.; Tong, H. In Situ Self-Sacrificed Template Synthesis of Fe-N/G Catalysts for Enhanced Oxygen Reduction. *ACS Appl. Mater. Interfaces* **2015**, *7*, 18170−18178.
[138] Sun, H.; Wang, M.; Du, X.; Jiao, Y.; Liu, S.; Qian, T.; Yan, Y.; Liu, C.; Liao, M.; Zhang, Q.; Meng, L.; Gu, L.; Xiong, J.; Yan, C. Modulating the d-band center of boron doped single-atom sites to boost the

oxygen reduction reaction. *J. Mater. Chem. A* **2019**, *7*, 20952−20957.
[139] Sun, T.; Zhao, S.; Chen, W.; Zhai, D.; Dong, J.; Wang, Y.; Zhang, S.; Han, A.; Gu, L.; Yu, R.; Wen, X.; Ren, H.; Xu, L.; Chen, C.; Peng, Q.; Wang, D.; Li, Y. Single-atomic cobalt sites embedded in hierarchically ordered porous nitrogen-doped carbon as a superior bifunctional electrocatalyst. *Proc. Natl. Acad. Sci. U. S. A.* **2018**, *115*, 12692−12697.
[140] Wu, K.; Chen, X.; Liu, S.; Pan, Y.; Cheong, W.-C.; Zhu, W.; Cao, X.; Shen, R.; Chen, W.; Luo, J.; Yan, W.; Zheng, L.; Chen, Z.; Wang, D.; Peng, Q.; Chen, C.; Li, Y. Porphyrin-like Fe-N4 sites with sulfur adjustment on hierarchical porous carbon for different rate-determining steps in oxygen reduction reaction. *Nano Res.* **2018**, *11*, 6260−6269.
[141] Hou, C.; Zou, L.; Sun, L.; Zhang, K.; Liu, Z.; Li, Y.; Li, C.; Zou, R.; Yu, J.; Xu, Q. Single-Atom Iron Catalysts on Overhang-Eave Carbon Cages for High-Performance Oxygen Reduction Reaction. *Angew. Chem. Int. Ed.* **2020**, *59*, 7384−7389.
[142] Yang, G.; Zhu, J.; Yuan, P.; Hu, Y.; Qu, G.; Lu, B. A.; Xue, X.; Yin, H.; Cheng, W.; Cheng, J.; Xu, W.; Li, J.; Hu, J.; Mu, S.; Zhang, J. N. Regulating Fe-spin state by atomically dispersed Mn-N in Fe-N-C catalysts with high oxygen reduction activity. *Nat. Commun.* **2021**, *12*, 1734.
[143] Chen, K.; Liu, K.; An, P.; Li, H.; Lin, Y.; Hu, J.; Jia, C.; Fu, J.; Li, H.; Liu, H.; Lin, Z.; Li, W.; Li, J.; Lu, Y. R.; Chan, T. S.; Zhang, N.; Liu, M. Iron phthalocyanine with coordination induced electronic localization to boost oxygen reduction reaction. *Nat. Commun.* **2020**, *11*, 4173.
[144] Zhang, X.; Zhang, S.; Yang, Y.; Wang, L.; Mu, Z.; Zhu, H.; Zhu, X.; Xing, H.; Xia, H.; Huang, B.; Li, J.; Guo, S.; Wang, E. A General Method for Transition Metal Single Atoms Anchored on Honeycomb-Like Nitrogen-Doped Carbon Nanosheets. *Adv. Mater.* **2020**, *32*, 1906905.
[145] Zhang, X.; Han, X.; Jiang, Z.; Xu, J.; Chen, L.; Xue, Y.; Nie, A.; Xie, Z.; Kuang, Q.; Zheng, L. Atomically dispersed hierarchically ordered porous Fe–N–C electrocatalyst for high performance electrocatalytic oxygen reduction in Zn-Air battery. *Nano Energy* **2020**, *71*, 104547.
[146] Liu, S.; Li, Z.; Wang, C.; Tao, W.; Huang, M.; Zuo, M.; Yang, Y.; Yang, K.; Zhang, L.; Chen, S.; Xu, P.; Chen, Q. Turning main-group element magnesium into a highly active electrocatalyst for oxygen reduction reaction. *Nat. Commun.* **2020**, *11*, 938.
[147] Jiang, Y.; Huang, L.; Chen, C.; Zheng, Y.; Qiao, S.-Z. Catalyst–electrolyte interface engineering propels progress in acidic CO_2 electroreduction. *Energy Environ. Sci.* **2025**, *18*, 2025–2049.
[148] Wang, J.; Zhang, J.; Chen, C. Electrochemical CO_2RR to C_{2+} products: A vision of dynamic surfaces of Cu-based catalysts. *Chin. J. Catal.* **2025**, *68*, 83–102.
[149] Li, J.; Abbas, S. U.; Wang, H.; Zhang, Z.; Hu, W. Recent Advances in Interface Engineering for Electrocatalytic CO_2 Reduction Reaction. *Nano-Micro Lett.* **2021**, *13*, 216.
[150] Yang, F.; Han, H.; Duan, H.; Fan, F.; Chen, S.; Bao, Y.; He, Y. L. A Review on Single Site Catalysts for Electrochemical CO_2 Reduction. *Adv. Energy Mater.* **2025**, *15*, 2405726.
[151] Zhu, Z.; Tang, W.; Wang, J.; Zhao, L.; Lin, Y.; Li, Z.; Niu, X.; Chen, J.; Wu, R. Insights into Operating Conditions on Electrocatalytic CO_2 Reduction. *Adv. Energy Mater.* **2025**, *15*, 2405769.
[152] Liu, M.; Hu, C.; Shen, K.; Chen, L.; Li, Y. Edge-hosted Fe single-atomic sites fabricated by a Bi-assisted pyrolysis strategy for electroreduction of CO_2. *Chem. Commun.* **2025**, *61*, 7081–7084.
[153] Wang, F.; Han, X.; Wu, D.; Wang, Z.; Xiong, X.; Li, J.; Gao, X.; Wang, G.; Huo, L.; Hua, Y.; Wang, C.; Wen, H.; Chen, Q.; Tian, X.; Deng, P. Electron Penetration Effect of Ni Single Atom Boosting CO_2 to CO in PH‐Universal Electrolytes. *Adv. Funct. Mater.* **2024**, *34*, 2314453.
[154] Wang, J.; Chen, X.; Yang, Z.; Xiao, J.-D.; Qin, C.; Yan, Z.; Wang, Z.; Yang, J.; Wang, J. Isolated cobalt–nitrogen sites on high-curvature carbon achieving industrial-level current density and pH-universal CO_2 electroreduction. *J. Mater. Chem. A* **2024**, *12*, 9147–9154.
[155] Tian, H.; Song, A.; Tian, H.; Liu, J.; Shao, G.; Liu, H.; Wang, G. Single-atom catalysts for high-energy rechargeable batteries. *Chem. Sci.* **2021**, *12*, 7656–7676.
[156] Zhang, Y.; Kang, C.; Zhao, W.; Song, Y.; Zhu, J.; Huo, H.; Ma, Y.; Du, C.; Zuo, P.; Lou, S.; Yin, G. d-p Hybridization-Induced "Trapping-Coupling-Conversion" Enables High-Efficiency Nb Single-Atom Catalysis for Li-S Batteries. *J. Am. Chem. Soc.* **2023**, *145*, 1728–1739.
[157] Chen, S.; Li, G.; Zhu, Z.; Zhu, R.; Zhang, J.; Yue, Y.; Li, G.; Zhou, L.; Yan, Z. Single-atom catalysts for lithium-sulfur batteries: Research progress and prospects. *J. Energy Chem.* **2025**, *107*, 440–458.
[158] Zhang, F.; Tang, Z.; Zheng, L.; Zhang, T.; Xu, M.; Xiao, H.; Zhuang, H.; Han, P.; Gao, Q. Edge-distributed iron single-atom moiety with efficient “trapping-conversion” for polysulfides driving high-performance of Li-S battery. *Appl. Catal. B: Environ.* **2023**, *334*, 122876.
[159] Jia, C.; Tan, X.; Zhao, Y.; Ren, W.; Li, Y.; Su, Z.; Smith, S.; Zhao, C. Sulfur-Dopant-Promoted Electroreduction of CO_2 over Coordinatively Unsaturated Ni-N_2 Moieties. *Angew. Chem. Int. Ed.* **2021**, *60*, 23342−23348.
[160] Sun, X.; Tuo, Y.; Ye, C.; Chen, C.; Lu, Q.; Li, G.; Jiang, P.; Chen, S.; Zhu, P.; Ma, M.; Zhang, J.; Bitter, J.; Wang, D.; Li, Y. Phosphorus Induced Electron Localization of Single Iron Sites for Boosted CO_2 Electroreduction Reaction. *Angew. Chem. Int. Ed.* **2021**, *60*, 23614−23618.
[161] Zhang, Z.; Zhu, J.; Chen, S.; Sun, W.; Wang, D. Liquid Fluxional Ga Single Atom Catalysts for Efficient Electrochemical CO_2 Reduction. *Angew. Chem. Int. Ed.* **2023**, *62*, e202215136.
[162] Wang, Q.; Dai, M.; Li, H.; Lu, Y. R.; Chan, T.-S.; Ma, C.; Liu, K.; Fu, J.; Liao, W.; Chen, S.; Pensa, E.; Wang, Y.; Zhang, S.; Sun, Y.; Cortes, E.; Liu, M. Asymmetric Coordination Induces Electron Localization at Ca Sites for Robust CO_2 Electroreduction to CO. *Adv. Mater.* **2023**, *35*, 2300695.
[163] Song, J.; Lei, X.; Mu, J.; Li, J.; Song, X.; Yan, L.; Ding, Y. Boron-Doped Nickel-Nitrogen-Carbon Single-Atom Catalyst for Boosting Electrochemical CO_2 Reduction. *Small* **2023**, *19*, 2305666.
[164] Dong, W.; Zhang, N.; Li, S.; Min, S.; Peng, J.; Liu, W.; Zhan, D.; Bai, H. A Mn single atom catalyst with Mn–N_2O_2 sites integrated into carbon nanosheets for efficient electrocatalytic CO_2 reduction. *J. Mater. Chem. A* **2022**, *10*, 10892−10901.
[165] Li, S.; Ceccato, M.; Lu, X.; Frank, S.; Lock, N.; Roldan, A.; Hu, X.-M.; Skrydstrup, T.; Daasbjerg, K. Incorporation of nickel single atoms into carbon paper as self-standing electrocatalyst for CO_2 reduction. *J. Mater. Chem. A* **2021**, *9*, 1583−1592.
[166] Li, Y.; Wei, B.; Zhu, M.; Chen, J.; Jiang, Q.; Yang, B.; Hou, Y.; Lei, L.; Li, Z.; Zhang, R.; Lu, Y. Synergistic Effect of Atomically Dispersed Ni-Zn Pair Sites for Enhanced CO_2 Electroreduction. *Adv. Mater.* **2021**, *33*, 2102212.
[167] Yun, R.; Zhan, F.; Wang, X.; Zhang, B.; Sheng, T.; Xin, Z.; Mao, J.; Liu, S.; Zheng, B. Design of Binary Cu-Fe Sites Coordinated with Nitrogen Dispersed in the Porous Carbon for Synergistic CO_2 Electroreduction. *Small* **2021**, *17*, 2006951.
[168] Jiao, L.; Zhu, J.; Zhang, Y.; Yang, W.; Zhou, S.; Li, A.; Xie, C.; Zheng, X.; Zhou, W.; Yu, S. H.; Jiang, H. L. Non-Bonding Interaction of Neighboring Fe and Ni Single-Atom Pairs on MOF-Derived N-Doped Carbon for Enhanced CO_2 Electroreduction. *J. Am. Chem. Soc.* **2021**, *143*, 19417−19424.
[169] Pei, J.; Wang, T.; Sui, R.; Zhang, X.; Zhou, D.; Qin, F.; Zhao, X.; Liu, Q.; Yan, W.; Dong, J.; Zheng, L.; Li, A.; Mao, J.; Zhu, W.; Chen, W.; Zhuang, Z. N-Bridged Co–N–Ni: new bimetallic sites for promoting electrochemical CO2 reduction. *Energy Environ. Sci.* **2021**, *14*, 3019−3028.
[170] Ren, W.; Tan, X.; Yang, W.; Jia, C.; Xu, S.; Wang, K.; Smith, S. C.; Zhao, C. Isolated Diatomic Ni-Fe Metal-Nitrogen Sites for Synergistic Electroreduction of CO_2. *Angew. Chem. Int. Ed.* **2019**, *58*, 6972−6976.
[171] Dhir, S.; Cattermull, J.; Jagger, B.; Schart, M.; Olbrich, L. F.; Chen, Y.; Zhao, J.; Sada, K.; Goodwin, A.; Pasta, M. Characterisation and modelling of potassium-ion batteries. *Nat. Commun.* **2024**, *15*, 7580.
[172] Li, M.; Wang, C.; Wang, C.; Lyu, Y.; Wang, J.; Xia, S.; Mao, J.; Guo, Z. 10 Years Development of Potassium-Ion Batteries. *Adv. Mater.* **2025**, *37*, 2416717.
[173] Igarashi, D.; Tanaka, Y.; Kubota, K.; Tatara, R.; Maejima, H.; Hosaka, T.; Komaba, S. New Template Synthesis of Anomalously Large Capacity Hard Carbon for Na‐ and K‐Ion Batteries. *Adv. Energy Mater.* **2023**, *13*, 2302647.
[174] Li, Y.; Zhu, A.; Peng, G.; He, J.; Li, H.; Jia, D.; Qiu, J.; He, X. Confined soft carbon in hard carbon with enhanced ion transport kinetics as anode for high-rate and stable potassium-ion batteries. *J. Energy Chem.* **2025**, *103*, 97–105.
[175] Xu, J.; Fan, C.; Ou, M.; Sun, S.; Xu, Y.; Liu, Y.; Wang, X.; Li, Q.; Fang, C.; Han, J. Correlation between Potassium-Ion Storage Mechanism and Local Structural Evolution in Hard Carbon Materials. *Chem. Mater.* **2022**, *34*, 4202–4211.
[176] Chen, Y.; Fu, N.; Shen, B.; Yan, Y.; Shao, W.; Wang, T.; Xie, H.; Yang, Z. Edge Coordination of Ni Single Atoms on Hard Carbon Promotes the Potassium Storage and Reversibility. *Small* **2023**, *19*, 2207423.
[177] Cheng, N.; Zhou, W.; Liu, J.; Liu, Z.; Lu, B. Reversible Oxygen-Rich Functional Groups Grafted 3D Honeycomb-Like Carbon Anode for Super-Long Potassium Ion Batteries. *Nano-Micro Lett.* **2022**, *14*, 146.
[178] Deng, H.; Wang, L.; Li, S.; Zhang, M.; Wang, T.; Zhou, J.; Chen, M.; Chen, S.; Cao, J.; Zhang, Q.; Zhu, J.; Lu, B. Radial Pores in Nitrogen/Oxygen Dual‐Doped Carbon Nanospheres Anode Boost High‐Power and Ultrastable Potassium‐Ion Batteries. *Adv. Funct. Mater.* **2021**, *31*, 2107246.
[179] Guo, Y.; Feng, Y.; Li, H.; Wang, Y.; Wen, Z.; Zhou, G. Carbon quantum dots in hard carbon: An approach to achieving PIB anodes with high potassium adsorption. *Carbon* **2022**, *189*, 142−151.
[180] Nam, K.-H.; Ganesan, V.; Chae, K. H.; Park, C.-M. High-performance carbon by amorphization and prepotassiation for potassium-ion battery anodes. *Carbon* **2021**, *181*, 290–299
[181] Yan, L.; Wang, J.; Ren, Q.; Fan, L.; Liu, B.; Zhang, L.; He, L.;

Mei, X.; Shi, Z. In-situ graphene-coated carbon microsphere as high initial coulombic efficiency anode for superior Na/K-ion full cell. *Chem. Eng. J.* **2022**, *432*, 133257.
[182] Zhang, W.; Sun, M.; Yin, J.; Lu, K.; Schwingenschlögl, U.; Qiu, X.; Alshareef, H. N. Accordion‐Like Carbon with High Nitrogen Doping for Fast and Stable K Ion Storage. *Adv. Energy Mater.* **2021**, *11*, 2101928.